Maxwell-consistent, symmetry- and energy-preserving solutions for ultrashort-laser-pulse propagation beyond the paraxial approximation

P. González de Alaiza Martínez,* G. Duchateau, B. Chimier, and R. Nuter
Centre Lasers Intenses et Applications, Université de Bordeaux-CNRS-CEA, UMR 5107, F-33405 Talence, France

I. Thiele
Department of Physics, Chalmers University of Technology, SE-412 96 Göteborg, Sweden

S. Skupin
Institut Lumière Matière, Université de Lyon-CNRS, UMR 5306, 69622 Villeurbanne, France

V. T. Tikhonchuk†
ELI-Beamlines, Institute of Physics, Czech Academy of Sciences, 25241 Dolní Břežany, Czech Republic

(Received 11 July 2018; published 29 October 2018)

We analytically and numerically investigate the propagation of ultrashort tightly focused laser pulses in vacuum, with particular emphasis on Hermite-Gaussian and Laguerre-Gaussian modes. We revisit the Lax series approach for forward-propagating linearly polarized laser pulses, to obtain Maxwell-consistent and symmetry-preserving analytical solutions for the propagation of all field components beyond the paraxial approximation in four-dimensional geometry (space and time). We demonstrate that our solution conserves the energy, which is set by the paraxial-level term of the series. The full solution of the wave equation towards which our series converges is calculated in the Fourier space. Three-dimensional numerical simulations of ultrashort tightly focused pulses validate our analytical development.

DOI: 10.1103/PhysRevA.98.043849

I. INTRODUCTION

Spatial and temporal pulse shaping makes the laser a highly versatile tool for a large number of applications such as micromachining and material processing [1–3], Terahertz generation [4,5], or biological imaging and noninvasive surgeries [6,7]. Paraxial approximation, which assumes that the light angular spectrum is sufficiently narrow, is widely used to study the propagation of laser beams in weak focusing conditions. However, the applications mentioned above usually require tightly focused ultrashort laser pulses. Modeling the propagation of such laser pulses is a complex problem because the deviation from the principal propagation direction is large and the paraxial approximation is no longer valid.

Electromagnetic codes, such as particle-in-cell codes [8,9] or codes based on the unidirectional pulse propagation equation [10,11], are powerful tools for understanding experiments on laser-matter interaction, where laser field components are commonly known in the far field. In these simulations external electromagnetic waves that enter the computational domain are usually prescribed as paraxial modes on the boundaries, which is not adequate for strongly focused ultrashort laser pulses because the initial distortion may be increased in the course of propagation [12], leading eventually to nonphysical fields in the simulation box. Therefore, there is a need to determine analytical solutions of Maxwell equations for tightly focused laser pulses.

Different analytical models, restricted to specific beam shapes or spatial symmetry conditions, have been developed to describe nonparaxial laser beam propagation in several physical contexts, such as perturbative expansions of the wave equation [13,14], the angular spectrum method [15], transformation optics [16], or analytical solutions based on the Helmholtz equation for laser-driven electron acceleration [17,18]. Lax *et al.* [19] proposed a simple method which paved the way to introduce the nonparaxial corrections to a given paraxial solution in more general situations. They demonstrated that the paraxial solution is actually the zeroth-order consistent solution to the Maxwell equations, obtained by expanding the wave equation (in their case, for a Gaussian linearly polarized vector potential) using a power series in the beam divergence angle.

The nonparaxial perturbative equations proposed by Lax *et al.* were subsequently analyzed in more detail, always on the basis of the wave equation applied to the vector potential, by several authors for either Gaussian beams [20–24] or Hermite-Gaussian and Laguerre-Gaussian beams [25–28]. Later, Porras *et al.* [29,30] proposed a similar time-domain perturbative approach, based on a different expansion parameter, to study the propagation of vectorial few-cycle light pulses. More recently, Favier *et al.* took into account spatiotemporal couplings in the wave equation to extend Lax perturbative equations to few-cycle pulses [31]. In the

*pedro.gonzalez@u-bordeaux.fr
†Also at Centre Lasers Intenses et Applications, Université de Bordeaux-CNRS-CEA, UMR 5107, F-33405 Talence, France.

transverse-spatial and temporal Fourier domain, they linked the Lax series with a Taylor expansion of the exact solution of the wave equation, but their proposed high-order corrections hinged on an arbitrary number of integration constants, which were chosen to match some known nonparaxial solutions.

This paper aims at addressing two problems which remain open despite the advances made in the previous works. The first problem is that all the previous approaches solely dealt with the wave equation (in the cited papers, applied to the vector potential) split into a Lax series, and not with the full set of Maxwell equations when calculating high-order corrections. Since each component of the electric, magnetic, and vector potential fields verifies the scalar wave equation, we expect to obtain a unique solution to the Maxwell equations whatever the component chosen to calculate high-order corrections. The second problem is that, when calculating high-order terms of the Lax series from the solutions at lower orders, spurious homogeneous solutions that are not compatible with Maxwell equations may be added through integration constants. We demonstrate in this paper that removing those spurious homogeneous solutions, as well as not breaking the existing symmetry between the electric and magnetic fields, makes preserving the laser energy through transverse planes possible. Conservation of energy is a fundamental physical principle that, to the best of our knowledge, had never been considered before in the context of nonparaxial corrections. Indeed, in previous works these integration constants were determined by making *ad hoc* assumptions, not sufficiently supported by the Maxwell equations, on how the nonparaxial corrections should be at the focal point [21,27] or on the beam axis [23].

In Sec. II, our Lax-series-based analytical solution for all electromagnetic field components is presented. Since Maxwell equations are satisfied, each electromagnetic field component verifies the scalar wave equation. By preserving the existing symmetry between the electric and magnetic fields, recursive relations to obtain the terms of our series are given in the Fourier space and the resulting solution is successfully compared with a numerically exact Maxwell solver [32]. Provided that there are no evanescent modes in the paraxial-level term, our solution is convergent. This solution as presented in Sec. II G represents an accurate way of injecting ultrashort laser pulses of arbitrary shape in space and time in codes based on the unidirectional pulse propagation equation and, under the cost of computing inverse Fourier transforms, also in finite-difference time-domain electromagnetic codes. In Sec. III we calculate the leading term of the asymptotic limit of our Lax-series-based analytical solution far from the focal plane, for both monochromatic beams and ultrashort laser pulses, which results in paraxial-like expressions. These analytical expressions are a baseline for further developments aiming at obtaining an easy and low-computational-cost means of computing the near fields related to those assumed-known paraxial far fields, avoiding the computation of any Fourier transform. Thanks to three-dimensional Maxwell-consistent numerical simulations carried out with the code ARCTIC, based on the Yee scheme [33], we discuss the adequacy of prescribing ultrashort laser pulses by the leading term of the asymptotic limit at a finite distance from the focal plane. Conclusions and outlooks are drawn in Sec. IV.

II. ANALYTICAL SOLUTIONS OF MAXWELL EQUATIONS

A. Maxwell equations and their properties

Maxwell equations in vacuum read as follows:

$$\boldsymbol{\nabla}\cdot\boldsymbol{E}=0, \tag{1}$$

$$\boldsymbol{\nabla}\cdot\boldsymbol{B}=0, \tag{2}$$

$$\partial_t\boldsymbol{B}+\boldsymbol{\nabla}\times\boldsymbol{E}=0, \tag{3}$$

$$\partial_t\boldsymbol{E}-c^2\boldsymbol{\nabla}\times\boldsymbol{B}=0, \tag{4}$$

where $\boldsymbol{E}$ and $\boldsymbol{B}$ are the electric and magnetic fields, respectively, and c is the speed of light in vacuum. Maxwell's equations are highly symmetrical and they place the electric and magnetic fields on equal footing [34]. Indeed, both electric and magnetic fields verify the wave equation:

$$\left(c^{-2}\partial_t^2-\boldsymbol{\nabla}^2\right)\boldsymbol{E}=\boldsymbol{0}, \tag{5}$$

$$\left(c^{-2}\partial_t^2-\boldsymbol{\nabla}^2\right)\boldsymbol{B}=\boldsymbol{0}. \tag{6}$$

Note that in this paper, we formally present our results in vacuum. For monochromatic or narrow-bandwidth pulses, by replacing c by c/n_0, where n_0 is a constant refractive index, our results generalize to homogeneous dielectric media. Because our solutions are derived in the Fourier space, it would be straightforward to extend it to shorter pulses with linear dispersion.

B. The wave equation

Throughout this paper, we shall work in Cartesian coordinates (x, y, z), where x is the optical propagation axis (also referred to as longitudinal axis) and y and z are the transverse coordinates. The beam focus position is placed at $x=0$.

We seek solutions of Maxwell equations that are waves propagating along longitudinal axis according to the following Ansatz:

$$\boldsymbol{E}(x,y,z,t)=E_0\begin{pmatrix}\psi_{E_x}(x,y,z,t)\\ \psi_{E_y}(x,y,z,t)\\ \psi_{E_z}(x,y,z,t)\end{pmatrix}e^{i(k_0x-\omega_0t)}, \tag{7}$$

$$\boldsymbol{B}(x,y,z,t)=\frac{E_0}{c}\begin{pmatrix}\psi_{B_x}(x,y,z,t)\\ \psi_{B_y}(x,y,z,t)\\ \psi_{B_z}(x,y,z,t)\end{pmatrix}e^{i(k_0x-\omega_0t)}, \tag{8}$$

where $\omega_0=2\pi c/\lambda_0$ is the angular frequency of the laser field, λ_0 is the wavelength, $k_0=\omega_0/c$ is the wave number, ψ_{E_x}, ψ_{E_y}, ψ_{E_z}, ψ_{B_x}, ψ_{B_y}, and ψ_{B_z} are the spatiotemporal envelopes of E_x, E_y, E_z, B_x, B_y, and B_z, respectively, and E_0 represents the electric field amplitude. Note that in this paper we only seek forward-propagating solutions propagating along x axis, as stated by Ansätze Eqs. (7) and (8), although Eqs. (5) and (6) admit, in general, bidirectional solutions. Implicitly, we require that $\boldsymbol{E}$ and $\boldsymbol{B}$ have no evanescent components. Moreover, because they are complex fields, the negative frequency

components are required to be the complex conjugates of their respective positive frequency components [35].

By substituting Eq. (7) into Eq. (5) and Eq. (8) into Eq. (6), each of the six spatial envelopes, generically denoted as ψ, verifies the so-called wave equation:

$$\boldsymbol{\nabla}_\perp^2\psi + 2ik_0\left[\partial_x + \frac{\partial_t}{c}\right]\psi = -\partial_x^2\psi + \frac{\partial_t^2\psi}{c^2}, \tag{9}$$

where $\boldsymbol{\nabla}_\perp^2 = \partial_y^2 + \partial_z^2$. It is useful to express Eq. (9) in the laser comoving reference system $x' = x$ and $t' = t - x/c$:

$$\boldsymbol{\nabla}_\perp^2\psi + 2ik_0\left(1 + \frac{i\partial_{t'}}{\omega_0}\right)\partial_{x'}\psi = -\partial_{x'}^2\psi. \tag{10}$$

The paraxial approximation neglects the term on the right-hand side of Eq. (10) by claiming that the field variation along x axis is small compared to the wavelength λ_0 (i.e., the wavefront is considered to be almost perpendicular to x axis) and to the transverse variation along y and z axes (i.e., the transverse profile is supposed to remain almost unchanged over a distance of the order of λ_0). Considering D_0 the $1/e$ diameter of the Gaussian solution in the beam focal plane (we assume that the diameter is the same along y and z axis) and $x_R = \pi D_0^2/(4\lambda_0)$ the associated Rayleigh length, we reformulate Eq. (10) in the dimensionless coordinates $\xi = x'/x_R$, $\tau = \omega_0 t'$, $\upsilon = 2y/D_0$, and $\zeta = 2z/D_0$ as follows:

$$\partial_\perp^2\psi + 4i\,T\,\partial_\xi\psi = -\varepsilon^2\partial_\xi^2\psi, \tag{11}$$

where $\partial_\perp^2 = \partial_\upsilon^2 + \partial_\zeta^2$ and the operator $T = 1 + i\,\partial_\tau$ introduces the space-time focusing [35,36]. Equation (11) reveals that the term on the right-hand side is actually a small correction of order of ε^2, where $\varepsilon = D_0/(2x_R)$ is the tangent of the beam divergence angle and is assumed to be small in the paraxial limit. For arbitrary spatial beam shapes, for which the Gaussian $1/e$ beam diameter D_0 does not apply, one can define ε as the angular spectral width divided by k_0. Note that monochromatic solutions are given by Eq. (11) in the limit $T \to 1$, which means that the time variation of the envelopes is negligible.

Equation (11) in the transverse-spatial and temporal Fourier domain (see Appendix A) reads:

$$\left(\frac{i\kappa_\perp^2}{4\hat{T}} + \partial_\xi - \frac{i\varepsilon^2}{4\hat{T}}\partial_\xi^2\right)\hat{\psi} = 0, \tag{12}$$

where $\kappa_\perp^2 = \kappa_y^2 + \kappa_z^2$, $\kappa_y = D_0k_y/2$, $\kappa_z = D_0k_z/2$, $\hat{T} = 1 + \Omega$, and $\Omega = \omega/\omega_0$. Restricting the temporal bandwidth of the complex fields $\boldsymbol{E}$ and $\boldsymbol{B}$ to the positive frequency range implies that $\Omega \ll 1$. The exact forward-propagating solution of Eq. (12), with the boundary condition placed at $\xi = 0$, reads:

$$\hat{\psi}(\xi,\kappa_y,\kappa_z,\Omega) = \hat{\psi}(0,\kappa_y,\kappa_z,\Omega)\,e^{-\frac{2i\hat{T}}{\varepsilon^2}\left(1-\sqrt{1-\frac{\varepsilon^2\kappa_\perp^2}{4\hat{T}^2}}\right)\xi}, \tag{13}$$

which, by abuse of language, will be called *general solution of the wave equation* all through this paper in spite of its lack of bidirectionality.

Equation (13) discloses that the exact forward-propagating solution preserves its complex module in all transverse planes:

$$|\hat{\psi}(\xi,\kappa_y,\kappa_z,\Omega)| = |\hat{\psi}(0,\kappa_y,\kappa_z,\Omega)|, \tag{14}$$

whenever $\varepsilon\kappa_\perp/(2\hat{T}) \leqslant 1$ (i.e., propagating modes).

C. The Lax series approach

A Taylor expansion of Eq. (13) in powers of $\kappa_\perp$ (around $\kappa_\perp = 0$) and ξ (around $\xi = 0$), reveals that the general solution of the wave equation depends on powers of ε [31]. Motivated by this fact, to solve Eq. (12) one can express $\hat{\psi}$ in a series using ε as expansion parameter [19]. Because this perturbative approach is a rearrangement of a Taylor expansion, its convergence is thus guaranteed by Taylor's theorem for any ε if high-order terms are calculated as explained below (i.e., satisfying Maxwell consistency, preserving the symmetry between electric and magnetic fields, and absence of evanescent modes). For linearly polarized laser pulses, the transverse components (i.e., $\hat{\psi}_{E_y}$, $\hat{\psi}_{E_z}$, $\hat{\psi}_{B_y}$, and $\hat{\psi}_{B_z}$, generically denoted as $\hat{\psi}_\perp$) expand in even powers of ε [20]:

$$\hat{\psi}_\perp(\xi,\kappa_y,\kappa_z,\Omega) = \sum_{j=0}^{\infty}\varepsilon^{2j}\hat{\psi}_\perp^{(2j)}(\xi,\kappa_y,\kappa_z,\Omega), \tag{15}$$

whereas the longitudinal components (i.e., $\hat{\psi}_{E_x}$ and $\hat{\psi}_{B_x}$, generically denoted as $\hat{\psi}_\parallel$) expand in odd powers of ε:

$$\hat{\psi}_\parallel(\xi,\kappa_y,\kappa_z,\Omega) = \sum_{j=0}^{\infty}\varepsilon^{2j+1}\hat{\psi}_\parallel^{(2j+1)}(\xi,\kappa_y,\kappa_z,\Omega), \tag{16}$$

where the functions $\hat{\psi}_\perp^{(2j)}$ and $\hat{\psi}_\parallel^{(2j+1)}$ have to be determined.

D. Lax series: Splitting the wave equation

If we substitute Eqs. (15) and (16) into Eq. (12), the wave equation is split into recursive equations. By doing so, the series Eqs. (15) and (16) satisfying the split Eqs. (17)–(20), respectively, will verify the wave Eq. (12) and hence will be completely equivalent to Eq. (13).

The lowest order ($j = 0$) corresponds to the paraxial equation:

$$\left(\frac{i\kappa_\perp^2}{4\hat{T}} + \partial_\xi\right)\hat{\psi}_\perp^{(0)} = 0, \tag{17}$$

$$\left(\frac{i\kappa_\perp^2}{4\hat{T}} + \partial_\xi\right)\hat{\psi}_\parallel^{(1)} = 0, \tag{18}$$

where $\hat{\psi}_\perp^{(0)} = C_{0,\perp}^{(0)}e^{-i\frac{\kappa_\perp^2}{4\hat{T}}\xi}$ and $\hat{\psi}_\parallel^{(1)} = C_{0,\parallel}^{(1)}e^{-i\frac{\kappa_\perp^2}{4\hat{T}}\xi}$ are, respectively, their solutions. The coefficients $C_{0,\perp}^{(0)} = C_{0,\perp}^{(0)}(\kappa_y,\kappa_z,\Omega)$ and $C_{0,\parallel}^{(1)} = C_{0,\parallel}^{(1)}(\kappa_y,\kappa_z,\Omega)$ do not depend on ξ (see their expressions for Hermite-Gaussian and Laguerre-Gaussian beams in Appendix B).

High-order corrections ($j > 0$) verify

$$\left(\frac{i\kappa_\perp^2}{4\hat{T}} + \partial_\xi\right)\hat{\psi}_\perp^{(2j)} = \frac{i}{4\hat{T}}\partial_\xi^2\hat{\psi}_\perp^{(2j-2)}, \tag{19}$$

$$\left(\frac{i\kappa_\perp^2}{4\hat{T}} + \partial_\xi\right)\hat{\psi}_\parallel^{(2j+1)} = \frac{i}{4\hat{T}}\partial_\xi^2\hat{\psi}_\parallel^{(2j-1)}, \tag{20}$$

with the paraxial differential operator in the left-hand side. We choose to express the solution to Eqs. (19) and (20) as the sum of a homogeneous solution $\hat{H}$ and a particular solution $\hat{P}$:

$$\hat{\psi}_{\perp}^{(2j)} = \hat{H}_{\perp}^{(2j)} + \hat{P}_{\perp}^{(2j)}, \tag{21}$$

$$\hat{\psi}_{\parallel}^{(2j+1)} = \hat{H}_{\parallel}^{(2j+1)} + \hat{P}_{\parallel}^{(2j+1)}, \tag{22}$$

where the homogeneous solutions are, respectively,

$$\hat{H}_{\perp}^{(2j)} = C_{0,\perp}^{(2j)} e^{-i\frac{\kappa_{\perp}^2}{4\hat{T}}\xi}, \tag{23}$$

$$\hat{H}_{\parallel}^{(2j+1)} = C_{0,\parallel}^{(2j+1)} e^{-i\frac{\kappa_{\perp}^2}{4\hat{T}}\xi}, \tag{24}$$

where the coefficients $C_{0,\perp}^{(2j)} = C_{0,\perp}^{(2j)}(\kappa_y, \kappa_z, \Omega)$ and $C_{0,\parallel}^{(2j+1)} = C_{0,\parallel}^{(2j+1)}(\kappa_y, \kappa_z, \Omega)$ do not depend on ξ. It is important to note that even though $\hat{H}_{\perp}^{(2j)}$ and $\hat{H}_{\parallel}^{(2j+1)}$ formally obey the paraxial equation, they are part of the nonparaxial high-order corrections.

The particular solutions can be written as

$$\hat{P}_{\perp}^{(2j)} = \mathcal{P}_{\perp}^{(2j)}(\xi) e^{-i\frac{\kappa_{\perp}^2}{4\hat{T}}\xi}, \tag{25}$$

$$\hat{P}_{\parallel}^{(2j+1)} = \mathcal{P}_{\parallel}^{(2j+1)}(\xi) e^{-i\frac{\kappa_{\perp}^2}{4\hat{T}}\xi}, \tag{26}$$

where the coefficients $\mathcal{P}_{\perp}^{(2j)}(\xi)$ and $\mathcal{P}_{\parallel}^{(2j+1)}(\xi)$ do depend on ξ. Since in the neighborhood of the focal plane the form $\hat{\psi} \sim e^{-i\frac{\kappa_{\perp}^2}{4\hat{T}}\xi}$ dominates, the particular solutions must vanish in that plane, i.e., $\mathcal{P}_{\perp}^{(2j)}(0) = \mathcal{P}_{\parallel}^{(2j+1)}(0) = 0$. To evaluate them through a recursive procedure as shown below, they can be constructed as j-order polynomials in ξ:

$$\mathcal{P}_{\perp}^{(2j)}(\xi) = \sum_{k=1}^{j} C_{k,\perp}^{(2j)} \xi^k, \tag{27}$$

$$\mathcal{P}_{\parallel}^{(2j+1)}(\xi) = \sum_{k=1}^{j} C_{k,\parallel}^{(2j+1)} \xi^k, \tag{28}$$

where the coefficients $C_{k,\perp}^{(2j)}$ and $C_{k,\parallel}^{(2j+1)}$ have to be determined.

From the point of view of Lax recursive equations, homogeneous solutions $\hat{H}$ are simply arbitrary integration constants and hence Eqs. (19) and (20) do not suffice to determine them. These homogeneous solutions *must* be determined from the Maxwell equations by respecting the existing symmetry between the electric and magnetic fields (see Sec. II E). We demonstrate in this paper that such Maxwell-consistent and symmetry-preserving calculation of the high-order corrections ensures that the overall laser energy through transverse planes is not increased by the Lax series terms of order $j > 0$ and remains positive. Therefore, it can be easily rescaled to the paraxial-order energy (see Sec. II H). This is a fundamental difference with respect to previous works, where, for example, to determine the high-order corrections, some authors had considered *ad hoc* assumptions such that they are zero at the beam focal point [21,27], they follow the structure of a spherical wave emanating from the beam focal point [23] or they must match some known nonparaxial solutions [31]. Indeed, in the particular solutions proposed by most of these works dealing with Hermite-Gaussian and Laguerre-Gaussian paraxial families, spurious homogeneous solutions are found when a Gram-Schmidt orthogonalization process is applied in the focal plane [37,38]. These spurious modes make the total power through transverse planes increase with ε [23], which is not physical.

When substituting Eq. (21) into Eq. (19), and Eq. (22) into Eq. (20), the following recursion relations are obtained for the coefficients of the particular solutions for all $1 \leqslant k \leqslant j$ and $j > 0$:

$$C_{k,\perp}^{(2j)} = -\frac{i\kappa_{\perp}^4}{64\,\hat{T}^3}\frac{C_{k-1,\perp}^{(2j-2)}}{k} + \frac{\kappa_{\perp}^2}{8\,\hat{T}^2} C_{k,\perp}^{(2j-2)} + \frac{i}{4\,\hat{T}}(k+1) C_{k+1,\perp}^{(2j-2)}, \tag{29}$$

$$C_{k,\parallel}^{(2j+1)} = -\frac{i\kappa_{\perp}^4}{64\,\hat{T}^3}\frac{C_{k-1,\parallel}^{(2j-1)}}{k} + \frac{\kappa_{\perp}^2}{8\,\hat{T}^2} C_{k,\parallel}^{(2j-1)} + \frac{i}{4\,\hat{T}}(k+1) C_{k+1,\parallel}^{(2j-1)}, \tag{30}$$

where, by notation convention, $C_{k,\perp}^{(2j-2)} = C_{k,\parallel}^{(2j-1)} = 0$ if $k = j$ and $C_{k+1,\perp}^{(2j-2)} = C_{k+1,\parallel}^{(2j-1)} = 0$ if $k \geqslant j-1$.

It is important to note that the above recursive relations involve the coefficients $C_{0,\perp}^{(2j-2)}$ and $C_{0,\parallel}^{(2j-1)}$ of the homogeneous solution, which will be determined from the Maxwell equations in the following Sec. II E.

E. Lax series: Splitting Maxwell equations

We split Maxwell equations by substituting the Lax expansion Eqs. (15) and (16), together with the Ansätze Eqs. (7) and (8), into Eqs. (1)–(4).

The envelopes of all the electromagnetic components at paraxial order ($j = 0$) must verify simultaneously the following overdetermined system of equations:

$$\hat{T}\,\hat{\psi}_{E_x}^{(1)} + \frac{\kappa_y}{2}\hat{\psi}_{E_y}^{(0)} + \frac{\kappa_z}{2}\hat{\psi}_{E_z}^{(0)} = 0, \tag{31}$$

$$\hat{T}\,\hat{\psi}_{B_x}^{(1)} + \frac{\kappa_y}{2}\hat{\psi}_{B_y}^{(0)} + \frac{\kappa_z}{2}\hat{\psi}_{B_z}^{(0)} = 0, \tag{32}$$

$$\hat{T}\,\hat{\psi}_{B_x}^{(1)} - \frac{\kappa_y}{2}\hat{\psi}_{E_z}^{(0)} + \frac{\kappa_z}{2}\hat{\psi}_{E_y}^{(0)} = 0, \tag{33}$$

$$\hat{\psi}_{B_y}^{(0)} + \hat{\psi}_{E_z}^{(0)} = 0, \tag{34}$$

$$\hat{\psi}_{B_z}^{(0)} - \hat{\psi}_{E_y}^{(0)} = 0, \tag{35}$$

$$\hat{T}\,\hat{\psi}_{E_x}^{(1)} + \frac{\kappa_y}{2}\hat{\psi}_{B_z}^{(0)} - \frac{\kappa_z}{2}\hat{\psi}_{B_y}^{(0)} = 0, \tag{36}$$

which has a unique solution whatever two components are prescribed [32]. In this paper, without loss of generality, we choose the paraxial-order electric field polarized along y axis (note that the solution for any other polarization angle can be

obtained by applying a rotation transformation):

$$\hat{\psi}_{E_y}^{(0)} = C\, e^{-i\frac{\kappa_\perp^2}{4\hat{T}}\xi}, \tag{37}$$

$$\hat{\psi}_{E_z}^{(0)} = 0, \tag{38}$$

where $C(\kappa_y, \kappa_z, \Omega)$ is a coefficient not depending on ξ. The rest of the components are then calculated from the system Eqs. (31)–(36):

$$\hat{\psi}_{E_x}^{(1)} = -\frac{\kappa_y}{2\hat{T}}\, C\, e^{-i\frac{\kappa_\perp^2}{4\hat{T}}\xi}, \tag{39}$$

$$\hat{\psi}_{B_x}^{(1)} = -\frac{\kappa_z}{2\hat{T}}\, C\, e^{-i\frac{\kappa_\perp^2}{4\hat{T}}\xi}, \tag{40}$$

$$\hat{\psi}_{B_y}^{(0)} = 0, \tag{41}$$

$$\hat{\psi}_{B_z}^{(0)} = C\, e^{-i\frac{\kappa_\perp^2}{4\hat{T}}\xi}. \tag{42}$$

Similarly, the envelopes at high orders ($j > 0$) must verify simultaneously the following overdetermined system of recursive equations:

$$2i\,\hat{T}\,\hat{\psi}_{E_x}^{(2j+1)} + i\kappa_y\hat{\psi}_{E_y}^{(2j)} + i\kappa_z\hat{\psi}_{E_z}^{(2j)} = -\partial_\xi\hat{\psi}_{E_x}^{(2j-1)}, \tag{43}$$

$$2i\,\hat{T}\,\hat{\psi}_{B_x}^{(2j+1)} + i\kappa_y\hat{\psi}_{B_y}^{(2j)} + i\kappa_z\hat{\psi}_{B_z}^{(2j)} = -\partial_\xi\hat{\psi}_{B_x}^{(2j-1)}, \tag{44}$$

$$\hat{T}\,\hat{\psi}_{B_x}^{(2j+1)} - \frac{\kappa_y}{2}\hat{\psi}_{E_z}^{(2j)} + \frac{\kappa_z}{2}\hat{\psi}_{E_y}^{(2j)} = 0, \tag{45}$$

$$\hat{\psi}_{B_y}^{(2j)} + \hat{\psi}_{E_z}^{(2j)} = \frac{\kappa_z}{2\hat{T}}\hat{\psi}_{E_x}^{(2j-1)} + \frac{i}{2\hat{T}}\partial_\xi\hat{\psi}_{E_z}^{(2j-2)}, \tag{46}$$

$$\hat{\psi}_{B_z}^{(2j)} - \hat{\psi}_{E_y}^{(2j)} = -\frac{\kappa_y}{2\hat{T}}\hat{\psi}_{E_x}^{(2j-1)} - \frac{i}{2\hat{T}}\partial_\xi\hat{\psi}_{E_y}^{(2j-2)}, \tag{47}$$

$$\hat{T}\,\hat{\psi}_{E_x}^{(2j+1)} + \frac{\kappa_y}{2}\hat{\psi}_{B_z}^{(2j)} - \frac{\kappa_z}{2}\hat{\psi}_{B_y}^{(2j)} = 0, \tag{48}$$

$$\hat{\psi}_{B_z}^{(2j)} - \hat{\psi}_{E_y}^{(2j)} = \frac{\kappa_z}{2\hat{T}}\hat{\psi}_{B_x}^{(2j-1)} + \frac{i}{2\hat{T}}\partial_\xi\hat{\psi}_{B_z}^{(2j-2)}, \tag{49}$$

$$\hat{\psi}_{B_y}^{(2j)} + \hat{\psi}_{E_z}^{(2j)} = \frac{\kappa_y}{2\hat{T}}\hat{\psi}_{B_x}^{(2j-1)} + \frac{i}{2\hat{T}}\partial_\xi\hat{\psi}_{B_y}^{(2j-2)}, \tag{50}$$

which allows us to calculate the homogeneous parts in Eqs. (21) and (22). Note that the particular solutions calculated in Sec. II D satisfy Eqs. (43)–(50). To determine a unique homogeneous solution, we have to account for the symmetry existing between the electric and magnetic fields. For forward-propagating linearly polarized pulses, by observing Eqs. (46) and (50) and Eqs. (47) and (49), we require that

$$\hat{H}_{B_y}^{(2j)} - \hat{H}_{E_z}^{(2j)} = 0, \tag{51}$$

$$\hat{H}_{B_z}^{(2j)} + \hat{H}_{E_y}^{(2j)} = 0, \tag{52}$$

which indeed is the opposite situation to the paraxial order [compare to Eqs. (34) and (35)]. *A posteriori*, we will demonstrate in Sec. II H that this symmetry condition prevents high-order corrections from increasing the total laser energy.

After some manipulations, taking into account that we have prescribed the transverse electric field as in Eqs. (37) and (38), we get the following homogeneous solution for orders $j > 0$:

$$C_{0,E_x}^{(2j+1)} = \frac{\kappa_\perp^2}{16\hat{T}^2}C_{0,E_x}^{(2j-1)} + \frac{i}{4\hat{T}}C_{1,E_x}^{(2j-1)}, \tag{53}$$

$$\begin{aligned} C_{0,E_y}^{(2j)} = {} & \frac{\kappa_z^2}{8\hat{T}^2}C_{0,E_y}^{(2j-2)} - \frac{\kappa_\perp^2}{16\hat{T}^2}C_{0,B_z}^{(2j-2)} \\ & - \frac{\kappa_y\kappa_z}{8\hat{T}^2}C_{0,E_z}^{(2j-2)} - \frac{i}{4\hat{T}}C_{1,B_z}^{(2j-2)}, \end{aligned} \tag{54}$$

$$\begin{aligned} C_{0,E_z}^{(2j)} = {} & \frac{\kappa_y^2}{8\hat{T}^2}C_{0,E_z}^{(2j-2)} + \frac{\kappa_\perp^2}{16\hat{T}^2}C_{0,B_y}^{(2j-2)} \\ & - \frac{\kappa_y\kappa_z}{8\hat{T}^2}C_{0,E_y}^{(2j-2)} + \frac{i}{4\hat{T}}C_{1,B_y}^{(2j-2)}, \end{aligned} \tag{55}$$

$$C_{0,B_x}^{(2j+1)} = \frac{\kappa_\perp^2}{16\hat{T}^2}C_{0,B_x}^{(2j-1)} + \frac{i}{4\hat{T}}C_{1,B_x}^{(2j-1)}, \tag{56}$$

$$C_{0,B_y}^{(2j)} = C_{0,E_z}^{(2j)}, \tag{57}$$

$$C_{0,B_z}^{(2j)} = -C_{0,E_y}^{(2j)}, \tag{58}$$

where $C_{1,E_x}^{(1)} = C_{1,B_x}^{(1)} = C_{1,B_y}^{(0)} = C_{1,B_z}^{(0)} = 0$ by notation convention.

In conclusion, by setting C in Eqs. (37) and (38) the nonparaxial solution can be calculated in the whole space thanks to the recursive formulas Eqs. (29) and (30) and Eqs. (53)–(58). By way of example, the correction at order $j = 1$ reads:

$$\hat{\psi}_{E_x}^{(3)} = \left[\frac{\kappa_\perp^2}{16\hat{T}^2} - \frac{i\kappa_\perp^4}{64\hat{T}^3}\xi\right]\hat{\psi}_{E_x}^{(1)}, \tag{59}$$

$$\hat{\psi}_{E_y}^{(2)} = \left[\frac{\kappa_z^2 - \kappa_y^2}{16\hat{T}^2} - \frac{i\kappa_\perp^4}{64\hat{T}^3}\xi\right]\hat{\psi}_{E_y}^{(0)} - \frac{\kappa_y\kappa_z}{8\hat{T}^2}\hat{\psi}_{E_z}^{(0)}, \tag{60}$$

$$\hat{\psi}_{E_z}^{(2)} = \left[\frac{\kappa_y^2 - \kappa_z^2}{16\hat{T}^2} - \frac{i\kappa_\perp^4}{64\hat{T}^3}\xi\right]\hat{\psi}_{E_z}^{(0)} - \frac{\kappa_y\kappa_z}{8\hat{T}^2}\hat{\psi}_{E_y}^{(0)}, \tag{61}$$

$$\hat{\psi}_{B_x}^{(3)} = \left[\frac{\kappa_\perp^2}{16\hat{T}^2} - \frac{i\kappa_\perp^4}{64\hat{T}^3}\xi\right]\hat{\psi}_{B_x}^{(1)}, \tag{62}$$

$$\hat{\psi}_{B_y}^{(2)} = \left[\frac{\kappa_y^2 - \kappa_z^2}{16\hat{T}^2} + \frac{i\kappa_\perp^4}{64\hat{T}^3}\xi\right]\hat{\psi}_{E_z}^{(0)} - \frac{\kappa_y\kappa_z}{8\hat{T}^2}\hat{\psi}_{E_y}^{(0)}, \tag{63}$$

$$\hat{\psi}_{B_z}^{(2)} = \left[-\frac{\kappa_z^2 - \kappa_y^2}{16\hat{T}^2} - \frac{i\kappa_\perp^4}{64\hat{T}^3}\xi\right]\hat{\psi}_{E_y}^{(0)} + \frac{\kappa_y\kappa_z}{8\hat{T}^2}\hat{\psi}_{E_z}^{(0)}. \tag{64}$$

F. Example: Monochromatic Hermite-Gaussian and Laguerre-Gaussian beams

We confront our Lax-series-based analytical solution to a numerical algorithm computing Maxwell-consistent solutions [32] (see Appendix D). To do so, monochromatic beams are considered (i.e., $\hat{T} \to 1$) and the coefficient $C(\kappa_y, \kappa_z, \Omega)$ in Eqs. (37)–(42) shall refer here to either a Hermite-Gaussian beam [see Eq. (B8)] or a Laguerre-Gaussian beam [see Eq. (B16)]. Since the Lax series originates from a Taylor expansion around the beam focus, the best way to proceed is to prescribe our analytical solution in the focal plane,

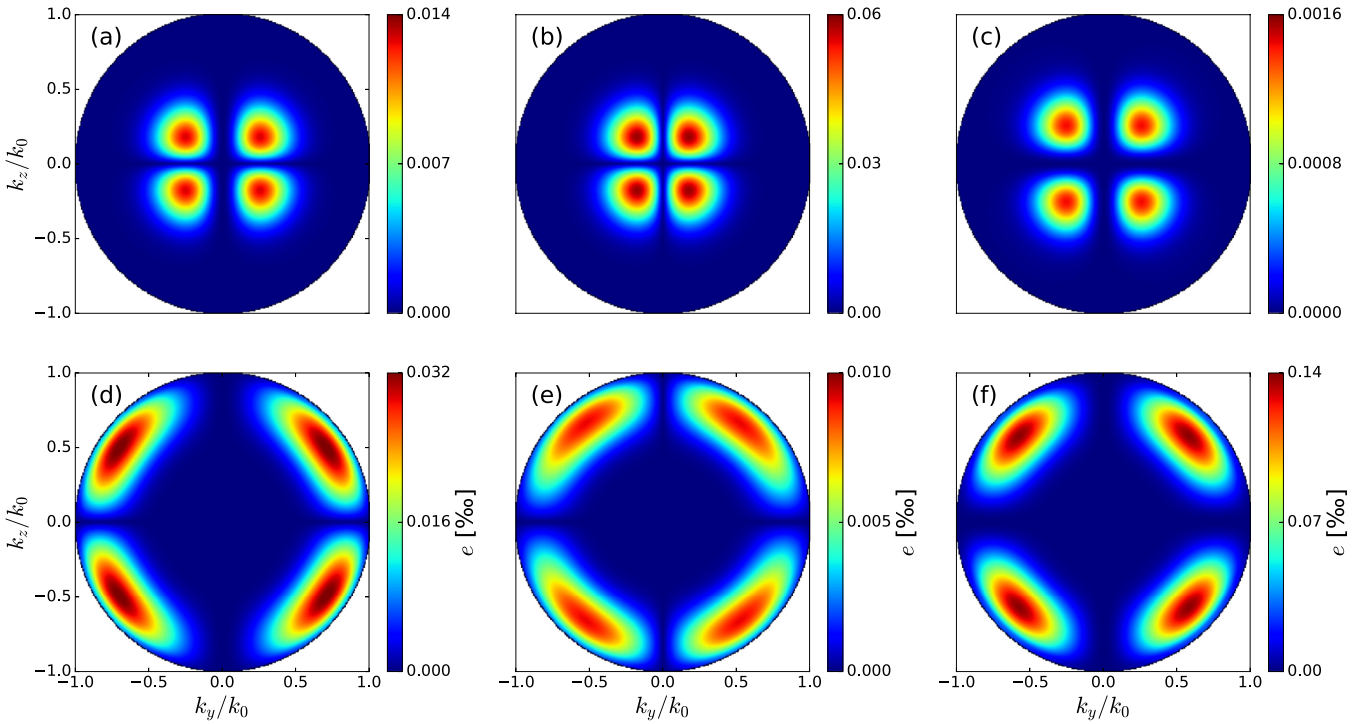

FIG. 1. Lax-series-based analytical solution $\hat{\psi}$ constructed from the (1,1)-order Hermite-Gaussian mode, truncated at order $j = 5$. We consider $\lambda_0 = 800\,\text{nm}$ and $\varepsilon = 0.25$. The results are plotted in the transverse plane placed at $\xi = 1$. We show the spatial envelopes for (a) E_x, (b) E_y, and (c) E_z. The corresponding local relative errors, given by Eq. (65), are shown in (d), (e), and (f), respectively.

truncated at different orders j, and subsequently measure, for all electromagnetic components, the error between the solution of the exact solver ($\hat{\psi}^{\text{solver}}$) and our analytical solution ($\hat{\psi}$) in different transverse planes. We compute errors using the standard Frobenius norm. The local relative error in a transverse plane is quantified as

$$e = e(\xi, \kappa_y, \kappa_z) = \frac{k_0\,|\hat{\psi}^{\text{solver}} - \hat{\psi}|}{\sqrt{\iint_{k_\perp^2 \leqslant k_0^2} |\hat{\psi}^{\text{solver}}|^2\,dk_y\,dk_z}}, \tag{65}$$

and the global relative error in the same plane is

$$\mathcal{E} = \mathcal{E}(\xi) = \sqrt{\frac{\iint_{k_\perp^2 \leqslant k_0^2} |\hat{\psi}^{\text{solver}} - \hat{\psi}|^2\,dk_y\,dk_z}{\iint_{k_\perp^2 \leqslant k_0^2} |\hat{\psi}^{\text{solver}}|^2\,dk_y\,dk_z}}. \tag{66}$$

Figures 1 and 2 show the analytical solution built from a (1,1)-order Hermite-Gaussian and (1,1)-order Laguerre-Gaussian modes, respectively, in the transverse plane placed at $\xi = 1$. We take $\lambda_0 = 800\,\text{nm}$ and a moderate $\varepsilon = 0.25$ (for which the evanescent power is negligible). The highest local relative error [see Eq. (65)] appear in a ring (i.e., high values of transverse wave numbers). When increasing the truncation order of the Lax series, this ring becomes narrower and the errors reduce in absolute value (not shown). This confirms numerically the convergence in the propagating region $k_\perp \leqslant k_0$ of our Lax-series-based solution seen as a Taylor expansion in κ_y and κ_z. Figure 3 shows that the global relative error diminishes too in all transverse planes when increasing the truncation order. This also confirms numerically the convergence in the propagating region of our Lax-series-based solution seen as a Taylor expansion in ξ. In the following Sec. II G we shall demonstrate that our solution converges by giving the limit of the series for the six electromagnetic field components.

G. Convergence of the solution

The Ansätze Eqs. (7) and (8) are substituted into the Maxwell Eqs. (1)–(4). In the transverse-spatial and temporal Fourier space, the resulting equations read

$$i\,\hat{T}\,\hat{\psi}_{E_x} + \frac{i\,\varepsilon\,\kappa_y}{2}\,\hat{\psi}_{E_y} + \frac{i\,\varepsilon\,\kappa_z}{2}\,\hat{\psi}_{E_z} = -\frac{\varepsilon^2}{2}\,\partial_\xi\hat{\psi}_{E_x}, \tag{67}$$

$$i\,\hat{T}\,\hat{\psi}_{B_x} + \frac{i\,\varepsilon\,\kappa_y}{2}\,\hat{\psi}_{B_y} + \frac{i\,\varepsilon\,\kappa_z}{2}\,\hat{\psi}_{B_z} = -\frac{\varepsilon^2}{2}\,\partial_\xi\hat{\psi}_{B_x}, \tag{68}$$

$$i\,\hat{T}\,\hat{\psi}_{B_x} - \frac{i\,\varepsilon\,\kappa_y}{2}\,\hat{\psi}_{E_z} + \frac{i\,\varepsilon\,\kappa_z}{2}\,\hat{\psi}_{E_y} = 0, \tag{69}$$

$$i\,\hat{T}\,\hat{\psi}_{E_x} + \frac{i\,\varepsilon\,\kappa_y}{2}\,\hat{\psi}_{B_z} - \frac{i\,\varepsilon\,\kappa_z}{2}\,\hat{\psi}_{B_y} = 0, \tag{70}$$

$$i\,\hat{T}\,\left(\hat{\psi}_{B_y} + \hat{\psi}_{E_z}\right) = \frac{i\,\varepsilon\,\kappa_z}{2}\,\hat{\psi}_{E_x} - \frac{\varepsilon^2}{2}\,\partial_\xi\hat{\psi}_{E_z}, \tag{71}$$

$$i\,\hat{T}\,\left(\hat{\psi}_{B_y} + \hat{\psi}_{E_z}\right) = \frac{i\,\varepsilon\,\kappa_y}{2}\,\hat{\psi}_{B_x} - \frac{\varepsilon^2}{2}\,\partial_\xi\hat{\psi}_{B_y}, \tag{72}$$

$$i\,\hat{T}\,\left(\hat{\psi}_{B_z} - \hat{\psi}_{E_y}\right) = -\frac{i\,\varepsilon\,\kappa_y}{2}\,\hat{\psi}_{E_x} + \frac{\varepsilon^2}{2}\,\partial_\xi\hat{\psi}_{E_y}, \tag{73}$$

$$i\,\hat{T}\,\left(\hat{\psi}_{B_z} - \hat{\psi}_{E_y}\right) = \frac{i\,\varepsilon\,\kappa_z}{2}\,\hat{\psi}_{B_x} - \frac{\varepsilon^2}{2}\,\partial_\xi\hat{\psi}_{B_z}, \tag{74}$$

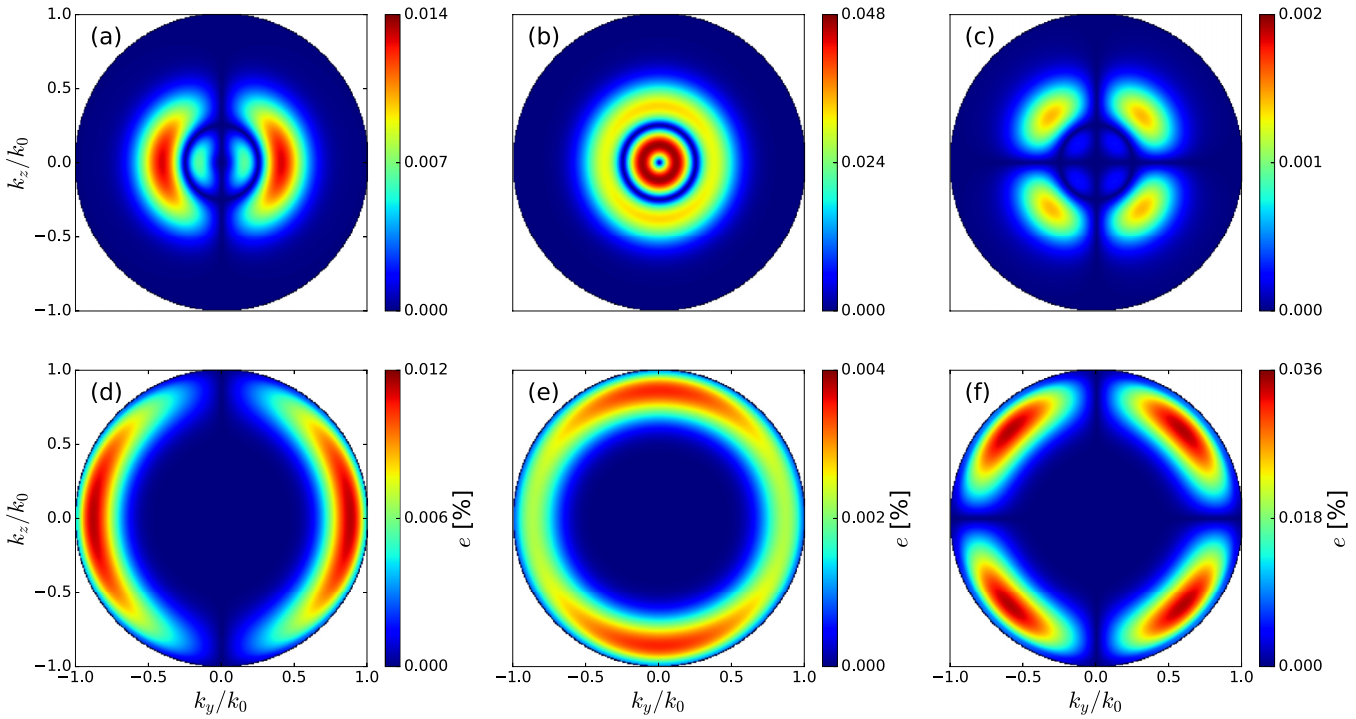

FIG. 2. Lax-series-based analytical solution $\hat{\psi}$ constructed from the (1,1)-order Laguerre-Gaussian mode, truncated at order $j = 5$. We consider $\lambda_0 = 800\,\text{nm}$ and $\varepsilon = 0.25$. The results are plotted in the transverse plane placed at $\xi = 1$. We show the spatial envelopes for (a) E_x, (b) E_y, and (c) E_z. The corresponding local relative errors, given by Eq. (65), are shown in (d), (e), and (f), respectively.

which, when they are split through Lax series Eqs. (15) and (16), encompass Eqs. (31)–(36) and Eqs. (43)–(50).

As explained in Sec. II D, each envelope in Eqs. (67)–(74) is assumed to be a forward-propagating solution of the wave Eq. (12), which is given by Eq. (13). After some manipulations, the substitution of Eq. (13), whose boundary condition is placed at $\xi = 0$, into Eqs. (67)–(74) yields

$$\frac{2}{\varepsilon}\,\hat{T}\,\mathcal{P}\,\hat{\psi}_{E_x}(0) + \kappa_y\,\hat{\psi}_{E_y}(0) + \kappa_z\,\hat{\psi}_{E_z}(0) = 0, \tag{75}$$

$$\frac{2}{\varepsilon}\,\hat{T}\,\mathcal{P}\,\hat{\psi}_{B_x}(0) + \kappa_y\,\hat{\psi}_{B_y}(0) + \kappa_z\,\hat{\psi}_{B_z}(0) = 0, \tag{76}$$

$$\frac{2}{\varepsilon}\,\hat{T}\,\hat{\psi}_{B_x}(0) - \kappa_y\,\hat{\psi}_{E_z}(0) + \kappa_z\,\hat{\psi}_{E_y}(0) = 0, \tag{77}$$

$$\frac{2}{\varepsilon}\,\hat{T}\,\hat{\psi}_{E_x}(0) + \kappa_y\,\hat{\psi}_{B_z}(0) - \kappa_z\,\hat{\psi}_{B_y}(0) = 0, \tag{78}$$

$$\frac{2}{\varepsilon}\,\hat{T}\,(1+\mathcal{P})\left[\hat{\psi}_{B_y}(0) + \hat{\psi}_{E_z}(0)\right] = \kappa_y\,\hat{\psi}_{B_x}(0) + \kappa_z\,\hat{\psi}_{E_x}(0), \tag{79}$$

$$\frac{2}{\varepsilon}\,\hat{T}\,(1+\mathcal{P})\left[\hat{\psi}_{B_z}(0) - \hat{\psi}_{E_y}(0)\right] = \kappa_z\,\hat{\psi}_{B_x}(0) - \kappa_y\,\hat{\psi}_{E_x}(0), \tag{80}$$

where $\hat{\psi}(0)$ refers to the value of the corresponding envelope in the focal plane and the operator $\mathcal{P}$ is given by

$$\mathcal{P} = \sqrt{1 - \frac{\varepsilon^2\,\kappa_\perp^2}{4\,\hat{T}^2}}, \tag{81}$$

where the argument of the square root must be nonnegative for forward-propagating waves (i.e., $\varepsilon\kappa_\perp/(2\hat{T}) \leqslant 1$). Therefore, $0 \leqslant \mathcal{P} \leqslant 1$, where the upper limit $\mathcal{P} \to 1$ represents the paraxial limit ($\varepsilon \to 0$).

Following Sec. II E, one needs to impose the symmetry condition Eqs. (51) and (52) to have a unique solution of

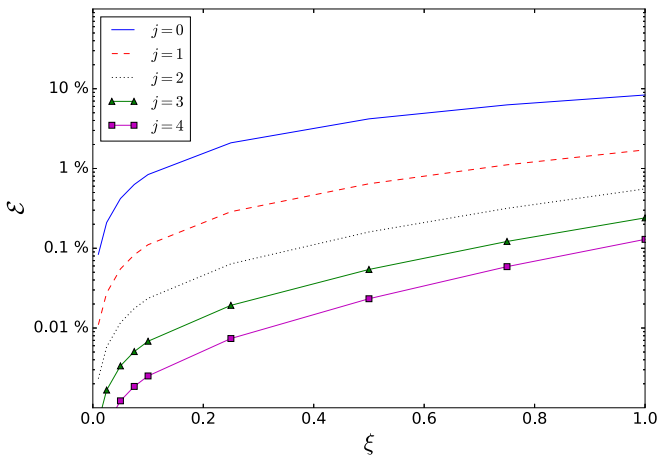

FIG. 3. Global relative error [Eq. (66)] between our analytical solution and the exact solution for E_y as a function of the longitudinal coordinate at different truncation orders. The Lax series is built from the (1,1)-order Hermite-Gaussian mode, taking $\lambda_0 = 800\,\text{nm}$ and $\varepsilon = 0.25$.

Eqs. (75)–(80). The values of the envelopes of the transverse field components in the focal plane are thus

$$\hat{\psi}_{E_y}(0) = C^{(0)}_{0,E_y} + \mathcal{H}_y, \tag{82}$$

$$\hat{\psi}_{B_z}(0) = C^{(0)}_{0,E_y} - \mathcal{H}_y, \tag{83}$$

$$\hat{\psi}_{E_z}(0) = C^{(0)}_{0,E_z} + \mathcal{H}_z, \tag{84}$$

$$\hat{\psi}_{B_y}(0) = -C^{(0)}_{0,E_z} + \mathcal{H}_z, \tag{85}$$

where the sum of the homogeneous parts of the high-order terms of the Lax series are

$$\mathcal{H}_y = \sum_{j=1}^{\infty} \varepsilon^{2j}\, C^{(2j)}_{0,E_y}, \tag{86}$$

$$\mathcal{H}_z = \sum_{j=1}^{\infty} \varepsilon^{2j}\, C^{(2j)}_{0,E_z}. \tag{87}$$

When inserting Eqs. (82)–(85) into Eqs. (75)–(80), a unique solution is obtained in terms of $C^{(0)}_{0,E_y}$ and $C^{(0)}_{0,E_z}$:

$$\mathcal{H}_y = -\frac{\varepsilon^2\left(\kappa_y^2-\kappa_z^2\right)}{4\,\hat{T}^2(1+\mathcal{P})^2}\, C^{(0)}_{0,E_y} - \frac{\varepsilon^2\,\kappa_y\kappa_z}{2\,\hat{T}^2(1+\mathcal{P})^2}\, C^{(0)}_{0,E_z}, \tag{88}$$

$$\mathcal{H}_z = \frac{\varepsilon^2\left(\kappa_y^2-\kappa_z^2\right)}{4\,\hat{T}^2(1+\mathcal{P})^2}\, C^{(0)}_{0,E_z} - \frac{\varepsilon^2\,\kappa_y\kappa_z}{2\,\hat{T}^2(1+\mathcal{P})^2}\, C^{(0)}_{0,E_y}, \tag{89}$$

which yields

$$\hat{\psi}_{E_y}(0) = \left[1 - \frac{\varepsilon^2\left(\kappa_y^2-\kappa_z^2\right)}{4\,\hat{T}^2(1+\mathcal{P})^2}\right] C^{(0)}_{0,E_y} - \frac{\varepsilon^2\,\kappa_y\kappa_z}{2\,\hat{T}^2(1+\mathcal{P})^2}\, C^{(0)}_{0,E_z}, \tag{90}$$

$$\hat{\psi}_{B_z}(0) = \left[1 + \frac{\varepsilon^2\left(\kappa_y^2-\kappa_z^2\right)}{4\,\hat{T}^2(1+\mathcal{P})^2}\right] C^{(0)}_{0,E_y} + \frac{\varepsilon^2\,\kappa_y\kappa_z}{2\,\hat{T}^2(1+\mathcal{P})^2}\, C^{(0)}_{0,E_z}, \tag{91}$$

$$\hat{\psi}_{E_z}(0) = \left[1 + \frac{\varepsilon^2\left(\kappa_y^2-\kappa_z^2\right)}{4\,\hat{T}^2(1+\mathcal{P})^2}\right] C^{(0)}_{0,E_z} - \frac{\varepsilon^2\,\kappa_y\kappa_z}{2\,\hat{T}^2(1+\mathcal{P})^2}\, C^{(0)}_{0,E_y}, \tag{92}$$

$$\hat{\psi}_{B_y}(0) = \left[-1 + \frac{\varepsilon^2\left(\kappa_y^2-\kappa_z^2\right)}{4\,\hat{T}^2(1+\mathcal{P})^2}\right] C^{(0)}_{0,E_z} - \frac{\varepsilon^2\,\kappa_y\kappa_z}{2\,\hat{T}^2(1+\mathcal{P})^2}\, C^{(0)}_{0,E_y}, \tag{93}$$

$$\hat{\psi}_{E_x}(0) = -\frac{\varepsilon}{\hat{T}(1+\mathcal{P})}\left[\kappa_y\, C^{(0)}_{0,E_y} + \kappa_z C^{(0)}_{0,E_z}\right], \tag{94}$$

$$\hat{\psi}_{B_x}(0) = -\frac{\varepsilon}{\hat{T}(1+\mathcal{P})}\left[\kappa_z\, C^{(0)}_{0,E_y} - \kappa_y C^{(0)}_{0,E_z}\right]. \tag{95}$$

The existence of the solutions Eqs. (90)–(95), which result in *finite* values for $0 \leqslant \mathcal{P} \leqslant 1$ (forward-propagating modes), implies that the Lax series obtained following our procedure is convergent, since these values actually represent the limit towards which our analytical solution converges in the focal plane.

Taking into account that paraxial-order terms follow Eq. (B2) and solutions of the wave equation are governed by Eq. (13), from Eqs. (90)–(95) one can express our solution as a function of the prescribed paraxial modes $\hat{\psi}^{(0)}_{E_y}$ and $\hat{\psi}^{(0)}_{E_z}$:

$$\hat{\psi}_{E_y} = \left[1 - \frac{\varepsilon^2\left(\kappa_y^2-\kappa_z^2\right)}{4\,\hat{T}^2(1+\mathcal{P})^2}\right] e^{-\frac{i\,\hat{T}(1-\mathcal{P})^2}{\varepsilon^2}\xi}\, \hat{\psi}^{(0)}_{E_y} - \frac{\varepsilon^2\,\kappa_y\kappa_z}{2\,\hat{T}^2(1+\mathcal{P})^2}\, e^{-\frac{i\,\hat{T}(1-\mathcal{P})^2}{\varepsilon^2}\xi}\, \hat{\psi}^{(0)}_{E_z}, \tag{96}$$

$$\hat{\psi}_{B_z} = \left[1 + \frac{\varepsilon^2\left(\kappa_y^2-\kappa_z^2\right)}{4\,\hat{T}^2(1+\mathcal{P})^2}\right] e^{-\frac{i\,\hat{T}(1-\mathcal{P})^2}{\varepsilon^2}\xi}\, \hat{\psi}^{(0)}_{E_y} + \frac{\varepsilon^2\,\kappa_y\kappa_z}{2\,\hat{T}^2(1+\mathcal{P})^2}\, e^{-\frac{i\,\hat{T}(1-\mathcal{P})^2}{\varepsilon^2}\xi}\, \hat{\psi}^{(0)}_{E_z}, \tag{97}$$

$$\hat{\psi}_{E_z} = \left[1 + \frac{\varepsilon^2\left(\kappa_y^2-\kappa_z^2\right)}{4\,\hat{T}^2(1+\mathcal{P})^2}\right] e^{-\frac{i\,\hat{T}(1-\mathcal{P})^2}{\varepsilon^2}\xi}\, \hat{\psi}^{(0)}_{E_z} - \frac{\varepsilon^2\,\kappa_y\kappa_z}{2\,\hat{T}^2(1+\mathcal{P})^2}\, e^{-\frac{i\,\hat{T}(1-\mathcal{P})^2}{\varepsilon^2}\xi}\, \hat{\psi}^{(0)}_{E_y}, \tag{98}$$

$$\hat{\psi}_{B_y} = \left[-1 + \frac{\varepsilon^2\left(\kappa_y^2-\kappa_z^2\right)}{4\,\hat{T}^2(1+\mathcal{P})^2}\right] e^{-\frac{i\,\hat{T}(1-\mathcal{P})^2}{\varepsilon^2}\xi}\, \hat{\psi}^{(0)}_{E_z} - \frac{\varepsilon^2\,\kappa_y\kappa_z}{2\,\hat{T}^2(1+\mathcal{P})^2}\, e^{-\frac{i\,\hat{T}(1-\mathcal{P})^2}{\varepsilon^2}\xi}\, \hat{\psi}^{(0)}_{E_y}, \tag{99}$$

$$\hat{\psi}_{E_x} = -\frac{\varepsilon\, e^{-\frac{i\,\hat{T}(1-\mathcal{P})^2}{\varepsilon^2}\xi}}{\hat{T}(1+\mathcal{P})}\left[\kappa_y\, \hat{\psi}^{(0)}_{E_y} + \kappa_z \hat{\psi}^{(0)}_{E_z}\right], \tag{100}$$

$$\hat{\psi}_{B_x} = -\frac{\varepsilon\, e^{-\frac{i\,\hat{T}(1-\mathcal{P})^2}{\varepsilon^2}\xi}}{\hat{T}(1+\mathcal{P})}\left[\kappa_z\, \hat{\psi}^{(0)}_{E_y} - \kappa_y \hat{\psi}^{(0)}_{E_z}\right]. \tag{101}$$

One can verify that a Taylor expansion in ε of Eqs. (96)–(101) yields the terms of our series presented in Secs. II D and II E.

Inversely, assuming known a full forward-propagating solution of Maxwell equations, the underlying paraxial level from which that solution is constructed through the Lax series can be easily determined from Eqs. (96) and (98):

$$\hat{\psi}^{(0)}_{E_y} = \left[\frac{1+\mathcal{P}}{2} + \frac{\varepsilon^2\,\kappa_y^2}{8\,\hat{T}^2\mathcal{P}}\right] e^{\frac{i\,\hat{T}(1-\mathcal{P})^2}{\varepsilon^2}\xi}\, \hat{\psi}_{E_y} + \frac{\varepsilon^2\,\kappa_y\kappa_z}{8\,\hat{T}^2\mathcal{P}}\, e^{\frac{i\,\hat{T}(1-\mathcal{P})^2}{\varepsilon^2}\xi}\, \hat{\psi}_{E_z}, \tag{102}$$

$$\hat{\psi}^{(0)}_{E_z} = \left[\frac{1+\mathcal{P}}{2} + \frac{\varepsilon^2\,\kappa_z^2}{8\,\hat{T}^2\mathcal{P}}\right] e^{\frac{i\,\hat{T}(1-\mathcal{P})^2}{\varepsilon^2}\xi}\, \hat{\psi}_{E_z} + \frac{\varepsilon^2\,\kappa_y\kappa_z}{8\,\hat{T}^2\mathcal{P}}\, e^{\frac{i\,\hat{T}(1-\mathcal{P})^2}{\varepsilon^2}\xi}\, \hat{\psi}_{E_y}, \tag{103}$$

which needs the boundary condition $\hat{\psi} \to 0$ and $\hat{\psi}_{\perp}^{(0)} \to 0$ at $\kappa_{\perp}/\hat{T} = 2/\varepsilon$ (i.e., the separation between propagating and evanescent modes, given by $\mathcal{P} \to 0$).

Equations (96)–(101) can be directly exploited to accurately inject tightly focused ultrashort laser pulses of arbitrary shape in space and time in Maxwell codes based on the unidirectional pulse propagation equation [10,11]. Under the cost of computing an inverse Fourier transform in the transverse space and time [32], these equations can also be used to prescribe the laser field under highly nonparaxial conditions on the boundaries of finite-difference time-domain (FDTD) codes such as particle-in-cell (PIC) ones [8,9]. Since the spectrum is analytically known everywhere, the most efficient fashion of Fourier-backtransforming Eqs. (96)–(101) is through inverse discrete Fourier transforms (IDFT) based on quadrature formulas (see Sec. III).

H. Energy conservation

The overall laser energy is calculated by integrating the longitudinal component of the Poynting vector (Π_x) over transverse coordinates and time (see Appendix C):

$$U = \frac{D_0^2}{4\,\omega_0} \iiint_{-\infty}^{+\infty} \Pi_x \; d\upsilon \, d\zeta \, d\tau, \tag{104}$$

where $\Pi_x = c^2 \varepsilon_0 (E_y \bar{B}_z - E_z \bar{B}_y)$. Taking into account the Ansätze Eqs. (7) and (8), the normalized total energy expresses in terms of the inner product between envelopes defined by Eq. (C5) as follows:

$$\frac{4\,\omega_0}{c\varepsilon_0 E_0^2 D_0^2}\, U = \langle \psi_{E_y}, \psi_{B_z} \rangle - \langle \psi_{E_z}, \psi_{B_y} \rangle. \tag{105}$$

When substituting the Lax series Eq. (15) into Eq. (105), the overall energy expands in powers of ε as follows:

$$\begin{aligned} \langle \psi_{E_y}, \psi_{B_z} \rangle - \langle \psi_{E_z}, \psi_{B_y} \rangle = & \sum_{j=0}^{\infty} \varepsilon^{2j} \sum_{\alpha=0}^{j} \langle \psi_{E_y}^{(2\alpha)}, \psi_{B_z}^{(2j-2\alpha)} \rangle \\ & - \sum_{j=0}^{\infty} \varepsilon^{2j} \sum_{\alpha=0}^{j} \langle \psi_{E_z}^{(2\alpha)}, \psi_{B_y}^{(2j-2\alpha)} \rangle. \end{aligned} \tag{106}$$

To demonstrate the energy conservation, we shall search for the least upper and lower bounds of the total energy. From Eq. (106) one easily deduces that the total energy is bounded from below by zero:

$$\langle \psi_{E_y}, \psi_{B_z} \rangle - \langle \psi_{E_z}, \psi_{B_y} \rangle \geqslant 0, \tag{107}$$

since, for forward-propagating waves, the total energy cannot be negative.

We shall seek the least upper bound for the total energy in the transverse-spatial and temporal Fourier space. Thanks to the Plancherel's theorem, the normalized overall energy Eq. (105) can be calculated in the Fourier space as follows:

$$\begin{aligned} & \frac{4\,\omega_0}{c\varepsilon_0 E_0^2 D_0^2}\, U \\ & = 8\pi^3 \iiint_{\frac{\varepsilon\kappa_{\perp}}{2\hat{T}} \leqslant 1} \left(\hat{\psi}_{E_y} \bar{\hat{\psi}}_{B_z} - \hat{\psi}_{E_z} \bar{\hat{\psi}}_{B_y} \right) d\kappa_y \, d\kappa_z \, d\Omega. \end{aligned} \tag{108}$$

From the solutions Eqs. (96)–(99) the integrand in Eq. (108) can be calculated in any transverse plane after some manipulations:

$$\begin{aligned} & \hat{\psi}_{E_y} \bar{\hat{\psi}}_{B_z} - \hat{\psi}_{E_z} \bar{\hat{\psi}}_{B_y} \\ & \quad = \left[1 - \left(\frac{1-\mathcal{P}}{1+\mathcal{P}} \right)^2 \right] \left(\hat{\psi}_{E_y}^{(0)} \bar{\hat{\psi}}_{B_z}^{(0)} - \hat{\psi}_{E_z}^{(0)} \bar{\hat{\psi}}_{B_y}^{(0)} \right). \end{aligned} \tag{109}$$

Since $0 \leqslant \mathcal{P} \leqslant 1$ for forward-propagating waves, then $0 \leqslant (1-\mathcal{P})/(1+\mathcal{P}) \leqslant 1$ and thus the coefficient in Eq. (109) verifies

$$0 \leqslant 1 - \left(\frac{1-\mathcal{P}}{1+\mathcal{P}} \right)^2 \leqslant 1. \tag{110}$$

When substituting Eqs. (109) and (110) into Eq. (108), one easily deduces that the total energy is bounded from above by the paraxial-order energy:

$$\langle \psi_{E_y}, \psi_{B_z} \rangle - \langle \psi_{E_z}, \psi_{B_y} \rangle \leqslant \langle \psi_{E_y}^{(0)}, \psi_{B_z}^{(0)} \rangle - \langle \psi_{E_z}^{(0)}, \psi_{B_y}^{(0)} \rangle, \tag{111}$$

because $\hat{\psi}_{E_y}^{(0)} \bar{\hat{\psi}}_{B_z}^{(0)} - \hat{\psi}_{E_z}^{(0)} \bar{\hat{\psi}}_{B_y}^{(0)} = |C_{0,E_y}^{(0)}|^2 + |C_{0,E_z}^{(0)}|^2 \geqslant 0$ everywhere.

Finally, from the bounds Eqs. (107) and (111) we conclude that our solution has a positive total energy, which is bounded from above for any ε. Hence, the solution can always be rescaled to the paraxial-order energy.

In conclusion, we have demonstrated that, when the terms in the Lax series are computed in the way presented in this paper, the paraxial level bounds from above the total energy and high-order corrections do not increase it. This is in complete agreement with the nature of the wave equation. By observing its solution Eq. (13), the energy is set when prescribing whatever two laser field components in a chosen transverse plane, e.g., in virtue of Eqs. (96) and (98) and Eqs. (102) and (103). Provided that $0 \leqslant \mathcal{P} \leqslant 1$ the propagation phase $\exp[-2i\,\hat{T}(1-\mathcal{P})\xi/\varepsilon^2]$ in Eq. (13), whose ε-dependent part is introduced in the Lax series by all the high-order corrections, models the transport of this amount of energy, which remains unchanged through any transverse plane. This is the reason why the ε-increasing-dependence of the total energy that comes out in previous works [23] is not physical: it reflects the presence of spurious modes that are adding energy artificially.

We note the analogy to perturbative expansions of the wave function in quantum mechanics [39,40]. The quantum wave function (here analogous to the total energy) is always normalized to unity, same as the lowest-order of its expansion, i.e., the unperturbed wave function (here analogous to the paraxial-level energy).

Since computing inverse Fourier transforms far from focal plane may be computationally expensive due to the large transverse-spatial windows involved, in the following Sec. III, we shall calculate the leading term of the asymptotic limit of our Lax-series-based analytical solution far from the focal plane and discuss the adequacy of using that limit as boundary condition for FDTD Maxwell solvers instead of the full solutions presented in Sec. II G.

III. ASYMPTOTIC BEHAVIOR FAR FROM FOCAL PLANE

Let us assume that, following Eqs. (37)–(42), the transverse field components at the paraxial order in the position space are

$$\psi_{E_y}^{(0)} = \psi^{(0)}, \tag{112}$$

$$\psi_{E_z}^{(0)} = 0. \tag{113}$$

The paraxial mode $\psi^{(0)}$, assumed to be forward-propagating and hence to have no evanescent components, expands in the limit $\xi \to \pm\infty$ as

$$\psi^{(0)} = \frac{1}{\xi^N}\left[a_0 + \frac{a_1}{\xi} + \frac{a_2}{\xi^2} + \cdots\right], \tag{114}$$

where $N > 0$ is the leading exponent of the asymptotic limit (in general, N is not necessarily an integer), which implies that $a_0 \neq 0$, and all coefficients $a_j = a_j(\upsilon, \zeta, \tau)$ do not depend on ξ. Equation (114) verifies the paraxial Eq. (B1):

$$\frac{\partial_\perp^2 a_0}{\xi^N} + \frac{\partial_\perp^2 a_1 - 4i\,T\,N a_0}{\xi^{N+1}} + \frac{\partial_\perp^2 a_2 - 4i\,T\,(N+1)a_1}{\xi^{N+2}} + \cdots = 0, \tag{115}$$

from where we deduce that

$$\partial_\perp^{2(j+1)} a_j = 0, \tag{116}$$

for all $j \geqslant 0$.

In the scope of this paper, we aim at calculating the asymptotic limit where $\xi \to \pm\infty$ of our solution, generically denoted as ψ^∞, only at the leading term $O(\xi^{-N})$. The particular solutions of high-order corrections for E_y and E_z components, given by Eq. (29), vanish by virtue of Eq. (116) at the leading order $O(\xi^{-N})$. Hence, only the homogeneous solutions of high-order corrections may contribute to the limit $\xi \to \pm\infty$, given by Eqs. (54) and (55), at such leading order $O(\xi^{-N})$. After some manipulations, the limits for the transverse components are, respectively,

$$\frac{\psi_{E_y}^\infty}{\psi^{(0)}} \sim 1 + \frac{1}{a_0}\sum_{j=1}^{\infty} \varepsilon^{2j} A_{E_y}^{(2j)}, \tag{117}$$

$$\frac{\psi_{E_z}^\infty}{\psi^{(0)}} \sim \frac{1}{a_0}\sum_{j=1}^{\infty} \varepsilon^{2j} A_{E_z}^{(2j)}, \tag{118}$$

where, from Eqs. (60) and (61) we obtain for $j = 1$:

$$A_{E_y}^{(2)} = \frac{\left(\partial_\upsilon^2 - \partial_\zeta^2\right)}{16\,T^2}\, a_0, \tag{119}$$

$$A_{E_z}^{(2)} = \frac{\partial_{\upsilon\zeta}^2}{8\,T^2}\, a_0, \tag{120}$$

and, from Eqs. (54), (55), and (116) we obtain the following recursive formulas for $j > 1$:

$$A_{E_y}^{(2j)} = -\frac{1}{8\,T^2}\left[\partial_\zeta^2 A_{E_y}^{(2j-2)} - \partial_{\upsilon\zeta}^2 A_{E_z}^{(2j-2)}\right], \tag{121}$$

$$A_{E_z}^{(2j)} = -\frac{1}{8\,T^2}\left[\partial_\upsilon^2 A_{E_z}^{(2j-2)} - \partial_{\upsilon\zeta}^2 A_{E_y}^{(2j-2)}\right]. \tag{122}$$

From Eqs. (117)–(122) we see that the leading terms of the limits of E_y and E_z where $\xi \to \pm\infty$ hinge upon the dominant coefficient a_0 in Eq. (114). The series in Eqs. (117) and (118) must be truncated at order $\sim O(\xi^{-N})$. These limits are first specified below for monochromatic (i.e., $T \to 1$) Hermite-Gaussian (Appendix E 1) and Laguerre-Gaussian (Appendix E 2) families. Then, these limits are calculated with a time envelope coupled to Hermite-Gaussian (Appendix E 3) and Laguerre-Gaussian beams (Appendix E 4).

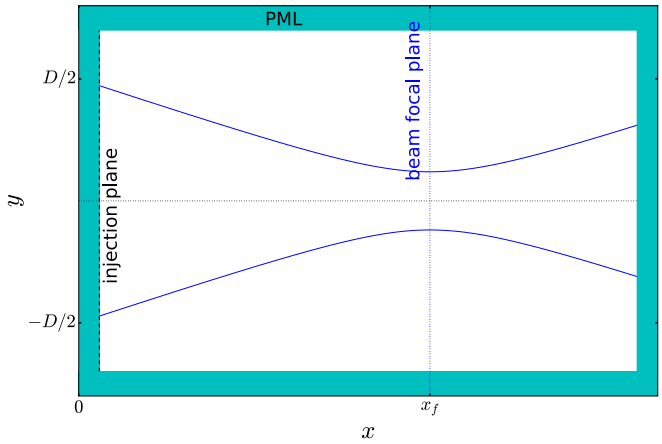

FIG. 4. Numerical box in ARCTIC (cut at $z = 0$). The PML region is colored in cyan. The parameters of the laser beam are defined at $x = 0$, namely, the $1/e$ diameter D and the numerical aperture. The injection plane for the total-field/scattered-field technique is placed right after the PML (vertical black dashed line). The beam focal plane (vertical blue dashed line) is at $x = x_f$. Solid blue lines illustrate the $1/e$ beam diameter of the corresponding Gaussian pulse.

As explained in Sec. II G, to carry out accurate simulations under highly nonparaxial conditions using FDTD Maxwell codes, computing inverse Fourier transforms of Eqs. (96)–(101) on boundaries is necessary [32]. Nevertheless, if the boundaries where fields need to be prescribed are very distant from the focal plane (several Rayleigh lengths), calculating inverse Fourier transforms would demand considerable computational resources because the transverse-spatial window is very large. Alternatively, since our analytical method is capable to link the nonparaxial near fields to the far fields through Eqs. (96)–(101), prescribing directly the leading term of the asymptotic limit *far enough from the focal plane* appears to be a reasonable simplification that helps us to save a big amount of computational resources in these kind of simulations up to a certain value of ε. Indeed, these leading terms in many cases are simply the paraxial-level term of the Lax series, as shown in Appendices E 1–E 4, and usually mimic quite well experimental conditions, e.g., a broad beam on a focusing mirror.

We verify our analytical results with three-dimensional (3D) Maxwell-consistent numerical simulations performed using the code ARCTIC [41]. Maxwell equations are discretized by means of Yee scheme [33]. The simulation domain is delimited by Bérenger's perfectly matched layer (PML) absorbing boundary condition [42,43]. The laser is injected via E_y, E_z, B_y, and B_z components in the transverse plane placed right after the PML according to the total-field/scattered-field technique [44], as shown in Fig. 4. This boundary is placed several Rayleigh lengths from the beam focus $x = x_f$.

The origin of the optical axis ($x = 0$) is set at the position of the left boundary. The input paraxial-order Gaussian pulse at $x = 0$ is characterized by its $1/e$ beam diameter D and numerical aperture (NA). The numerical aperture ($0 \leqslant \mathrm{NA} \leqslant 1$) of a Gaussian beam is defined as the sine of its divergence angle. Our Lax series expansion parameter $\varepsilon = (D_0/2)/x_R$, that is, the ratio of the $1/e$ beam radius at focus $D_0/2$ and the Rayleigh length x_R, represents the tangent of the beam divergence angle. Thus, expressed in terms of ε, the numerical aperture reads

$$\mathrm{NA} = \frac{\varepsilon}{\sqrt{1+\varepsilon^2}}. \tag{123}$$

The beam focal plane is situated at $x = x_f$:

$$x_f = \frac{\lambda_0}{\pi\varepsilon^2}\sqrt{\left(\frac{\pi\varepsilon D}{2\lambda_0}\right)^2 - 1}. \tag{124}$$

If injecting the leading term of the asymptotic expansion of our solution at $x = 0$ (i.e., a simple Gaussian beam) instead of directly injecting the Fourier-back-transformed full solution Eqs. (96)–(101), then the position of the focal plane obtained with the full Maxwell solver may differ from x_f due to simplifying high-order terms where $\xi \to \pm\infty$ in Eqs. (117)–(118).

We simulate a y-polarized Gaussian laser beam at the wavelength $\lambda_0 = 0.8\,\mu$m coupled, according to Eq. (E22), with the Gaussian time envelope:

$$C_\tau(\Omega) = \frac{\tau_p}{2\sqrt{\pi}} e^{-\frac{\tau_p^2\Omega^2}{4}} = \mathcal{F}_\tau\left[e^{-\frac{\tau^2}{\tau_p^2}}\right], \tag{125}$$

where $\tau_p = 16.99\,$fs is the $1/e$ duration and thus the full-width-at-half-maximum (FWHM) duration of the pulse (envelope of intensity) is 20 fs (i.e., 7.49 optical cycles). The $1/e$ beam diameter at $x = 0$ is $D = 7.31\,\mu$m. We take a numerical aperture of NA $= 0.57$ in the vacuum, which gives $\varepsilon = 0.7$ corresponding to strong focusing conditions where the nonparaxial regime is completely established [23]. The beam focal plane should be situated at $x_f = 5.20\,\mu$m according to Eq. (124). Since $x_R = 0.52\,\mu$m, the prescription plane is $x_f/x_R = 10$ Rayleigh lengths far from the beam focal plane. An overall input energy of 36 nJ is considered (which corresponds to $E_0 = 55.36\,\mathrm{GV/m}$). The resolution chosen in ARCTIC is $\Delta x = 31.8\,$nm (25 points per wavelength), $\Delta y = \Delta z = 63.7\,$nm (13 points per wavelength), and $\Delta t = 84.9\,$as (31 points per period). The PML layer is ten cells wide in each direction.

Figure 5 shows the maximum value of $|E_y|$ over time in the XY plane (i.e., $z = 0$). The laser pulse is prescribed according to Eq. (E22). The temporal inverse Fourier transformed is computed from Eq. (A6) using the 64-point Gauss-Legendre quadrature formula in the frequency interval $-10/\tau_p \leqslant \Omega \leqslant 10/\tau_p$. The error of 22% between the position of the beam focal plane given by ARCTIC ($x = 4.06\,\mu$m) and the theory ($x_f = 5.20\,\mu$m) is due to the fact that only the leading term of the asymptotic solution is taken into consideration. The previous evaluations have been performed within conditions of very tightly focused pulses ($\varepsilon = 0.7$). By decreasing ε to 0.5, the error drops to roughly 10% (not shown), which is

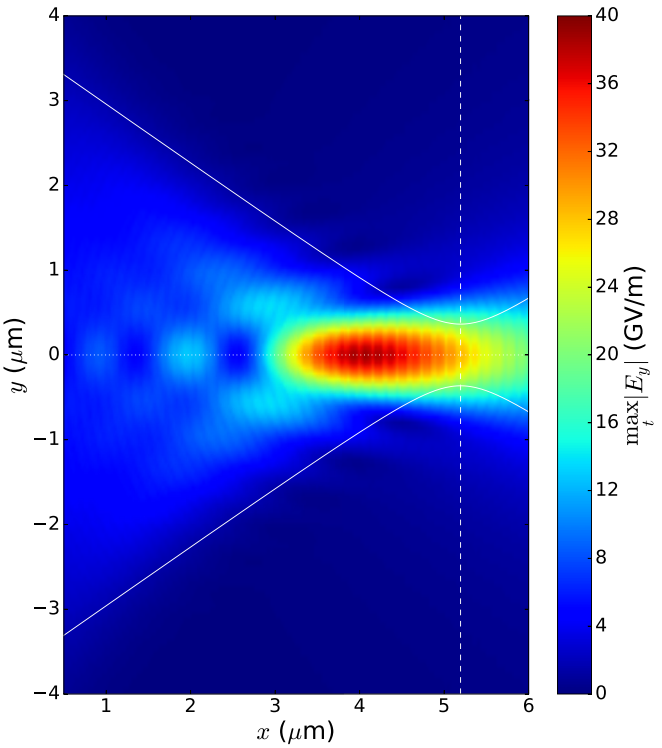

FIG. 5. Maximum value that $|E_y|$ reaches on the XY plane, for a y-polarized 0.8-μm-wavelength 20-fs-FWHM 36-nJ Gaussian laser beam prescribed at $x = 0$ with NA $= 0.57$ and $D = 7.31\,\mu$m. The horizontal white dotted line represents the optical axis. The length of the PML layer is $0.32\,\mu$m along x axis and hence the laser pulse is injected at $x = 0.32\,\mu$m using the paraxial-order term. The vertical white dashed line indicates the beam focal plane position ($x_f = 5.20\,\mu$m) and the white solid lines depict the profile of the Gaussian pulse (paraxial-order term of the Lax series). The leading term of the asymptotic expansion, given by Eq. (E22), is employed to prescribe the laser pulse.

acceptable. Therefore, it turns out that prescribing the laser fields at a *finite* distance implies a contribution of next-to-leading orders of the asymptotic expansion: the smaller ε, the smaller the next-to-leading order contribution.

The maximum values in the focal plane over time of the module of the electric field components are comparable with the module of the corresponding spatial envelopes with $T \to 1$. These latter values, $|E_0\psi|$, computed by Fourier-back-transforming Eqs. (96)–(101) with $\hat{T} = 1$, are depicted in Figs. 6(d)–6(f). A 64×64-point Gauss-Legendre quadrature formula in the transverse-wave-vector region $\kappa_\perp \leqslant 2/\varepsilon$ (i.e., the evanescent modes are filtered out) is used to compute the inverse discrete Fourier transforms via Eq. (A4). The peak of E_y predicted by our Lax-series-based solution is $48.26\,\mathrm{GV/m}$, which is lower than the peak of the paraxial-order term of the series ($E_0 = 55.36\,\mathrm{GV/m}$), as illustrated in Fig. 7, due to the strong focusing conditions. The cuts in the focal plane of the simulation corresponding to Fig. 5 are shown in Figs. 6(a)–6(c). One observes that the results of ARCTIC and our analytical solution qualitatively agree but the amplitudes are ∼20% smaller (the peak of E_y is $37.80\,\mathrm{GV/m}$).

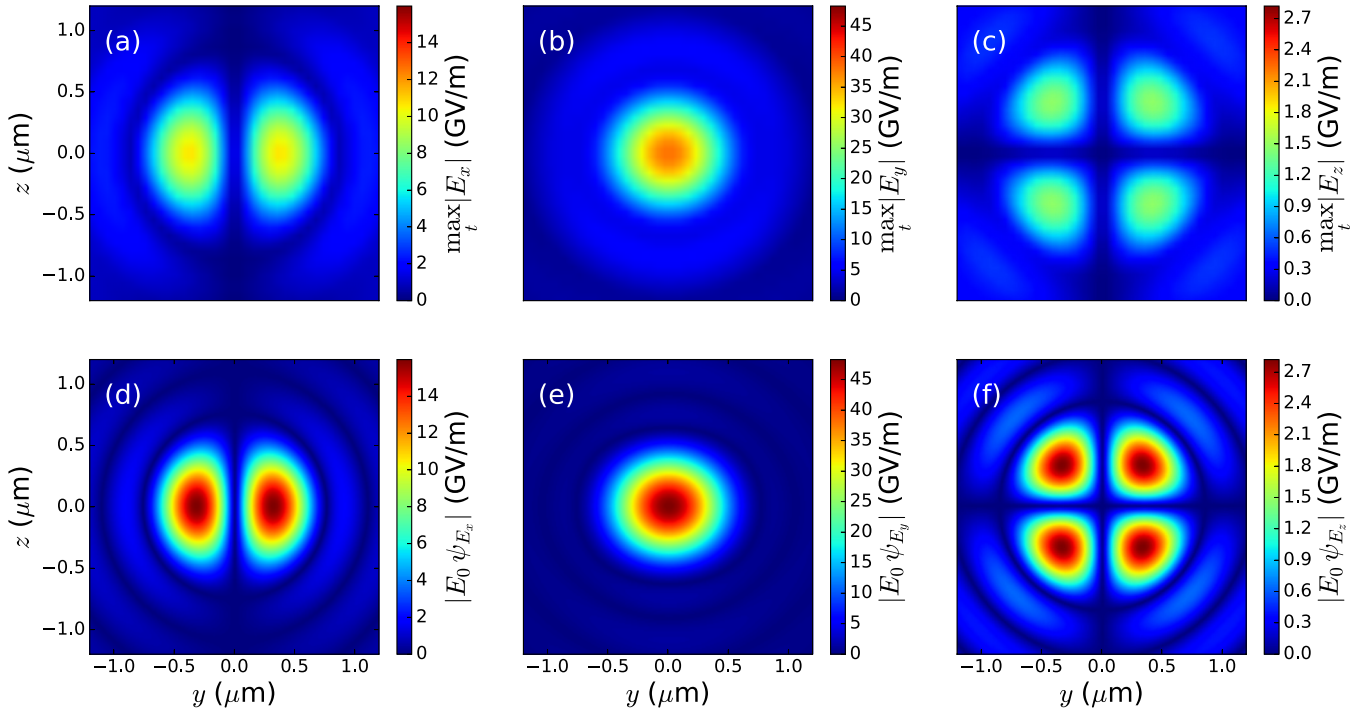

FIG. 6. Comparison of ARCTIC's results (maximum values that the module of the electric field components attain in the focal plane) with our analytical solution. Results corresponding to Fig. 5 in the beam focal plane at $x = 4.06\,\mu$m: Maximum values of (a) $|E_x|$, (b) $|E_y|$, and (c) $|E_z|$. Analytical solution in the focal plane at $x_f = 5.20\,\mu$m, calculated from Fourier-back-transformed Eqs. (96)–(101), with $T = 1$ and by filtering the evanescent modes: (d) $|E_0\,\psi_{E_x}|$, (e) $|E_0\,\psi_{E_y}|$, and (f) $|E_0\,\psi_{E_z}|$.

IV. CONCLUSION AND OUTLOOKS

Both the wave equation and the paraxial equation possess an infinite number of solutions. In this paper, we have demonstrated that from any paraxial solution we can build, in a self-consistent fashion, an exact solution of the wave equation for the six electromagnetic field components, assuming forward-propagating linearly-polarized laser pulses, which is consistent with Maxwell equations, conserves the energy transported through transverse planes, and preserves the symmetry between the electric and magnetic fields. To do so, we have split, following the procedure by Lax *et al.* [19] and in the transverse-spatial and temporal Fourier space, both the scalar wave equations applied to each electromagnetic field component and to the Maxwell equations. High-order corrections have been separated in a *homogeneous* solution and a *particular* solution. The particular solution is integrated directly from the wave equation. The homogeneous solution, instead, must be calculated so that the whole set of Maxwell equations is satisfied and the existing symmetry between the electric and magnetic fields is preserved. Only then the total laser energy through transverse planes is bounded for any ε. The fact that high-order corrections reduce the energy and make rescaling necessary implies that tight focusing leads necessarily to mode mixing with an ε-dependence of the number of active modes. We give simple recursive relations to obtain these Maxwell-consistent high-order corrections, which are polynomials on the longitudinal coordinate whose coefficients are paraxial modes related to transverse-spatial and temporal derivatives of the paraxial-order term of the Lax series. The convergence of our solution is demonstrated by giving the limits of the series in the transverse-spatial and temporal Fourier space. These limits are of direct application to accurately prescribe tightly-focused ultrashort laser pulses in Maxwell codes.

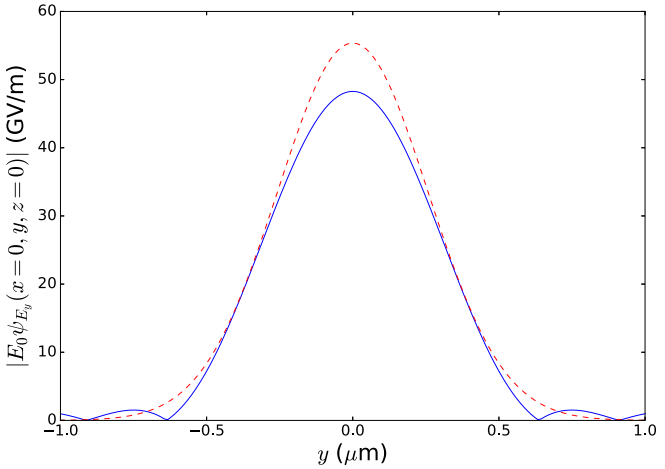

FIG. 7. Cut along y axis of $|E_0\,\psi_{E_y}|$ corresponding to Fig. 6(e) (blue solid line). The (upper) red dashed line accounts for the paraxial-order term of the series.

Since in experiments fields are usually known far from the focal plane, we have derived the leading term if the asymptotic expansion of the full analytical solution of the Maxwell equations. In the case of a strongly focused 20-fs-FWHM Gaussian laser pulse, numerical simulations confirm

the reliability of this asymptotic expression up to an accuracy of 10%. Further developments for next-to-leading orders are expected to decrease this error.

ACKNOWLEDGMENTS

This research was supported by the project ASTGV (Amplitude Systèmes Through-Glass Via) from French DGA (Direction Générale de l'Armement) funding, and also by the project ELITAS (ELI Tools for Advanced Simulation) CZ.02.1.01/0.0/0.0/16_013/0001793 from European Regional Development Fund. This work was granted access to the HPC resources of TGCC under the allocation A0030506129 made by GENCI and the allocation 2017174175 made by PRACE. S. Skupin acknowledges support by the Qatar National Research Fund (Grant No. NPRP 8-246-1-060). The authors are deeply grateful to the referee for his/her constructive input.

APPENDIX A: DEFINITION OF THE TRANSVERSE-SPATIAL AND TEMPORAL FOURIER TRANSFORM

Using the dimensionless coordinates $\xi = x'/x_R$, $\upsilon = 2y/D_0$, $\zeta = 2z/D_0$, $\kappa_y = D_0 k_y/2$, $\kappa_z = D_0 k_z/2$, $\tau = \omega_0 t'$, and $\Omega = \omega/\omega_0$ we define the transverse-spatial and temporal Fourier transform of ψ, denoted as $\hat{\psi}$, as the combination of the transverse-spatial Fourier transform ($\mathcal{F}_\perp$) and the temporal Fourier transform ($\mathcal{F}_\tau$):

$$\hat{\psi}(\xi, \kappa_y, \kappa_z, \Omega) = \mathcal{F}_\tau[\mathcal{F}_\perp[\psi(\xi, \upsilon, \zeta, \tau)]], \tag{A1}$$

$$\psi(\xi, \upsilon, \zeta, \tau) = \mathcal{F}_\tau^{-1}[\mathcal{F}_\perp^{-1}[\hat{\psi}(\xi, \kappa_y, \kappa_z, \Omega)]], \tag{A2}$$

where the transverse-spatial Fourier transform is

$$\mathcal{F}_\perp[\psi] = \frac{1}{4\pi^2} \iint \psi\, e^{-i(\kappa_y \upsilon + \kappa_z \zeta)}\, d\upsilon\, d\zeta, \tag{A3}$$

$$\psi = \iint \mathcal{F}_\perp[\psi]\, e^{i(\kappa_y \upsilon + \kappa_z \zeta)}\, d\kappa_y\, d\kappa_z, \tag{A4}$$

and the temporal Fourier transform is

$$\mathcal{F}_\tau[\psi] = \frac{1}{2\pi} \int \psi\, e^{i\Omega\tau}\, d\tau, \tag{A5}$$

$$\psi = \int \mathcal{F}_\tau[\psi]\, e^{-i\Omega\tau}\, d\Omega. \tag{A6}$$

For monochromatic pulses, the temporal Fourier transform defined in Eq. (A5) reduces to a multiplication by a Dirac δ function $\delta(\Omega)$ in the temporal Fourier space.

APPENDIX B: SOLUTIONS OF THE PARAXIAL EQUATIONS

The paraxial equation is

$$\left(\partial_\upsilon^2 + \partial_\zeta^2 + 4i\, T\, \partial_\xi\right)\psi = \left(\partial_\upsilon^2 + \partial_\zeta^2 + 4F^2\, T\, \partial_F\right)\psi = 0, \tag{B1}$$

where the complex longitudinal variable $F = i/(i - \xi)$ has already been introduced by Salamin [23]. By rewriting Eq. (B1) in the transverse-spatial and temporal Fourier space, we can see that the paraxial solution is of the form

$$\hat{\psi} = C(\kappa_y, \kappa_z, \Omega)\, e^{-i\frac{\kappa_\perp^2}{4T}\xi}, \tag{B2}$$

where $\kappa_\perp^2 = \kappa_y^2 + \kappa_z^2$ and $C(\kappa_y, \kappa_z, \Omega)$ is a coefficient independent of ξ.

Three families of exact solutions for Eq. (B1) are known when $T \to 1$ (i.e., monochromatic pulses): Hermite-Gaussian modes (often called the *free-space eigenmodes*), Laguerre-Gaussian modes, and Ince-Gaussian modes [45]. Each of these families constitute a countably infinite set of orthogonal paraxial solutions, and they are complete [26].

1. Hermite-Gaussian modes

The Hermite-Gaussian modes are a well-known complete family of orthogonal paraxial solutions:

$$\psi_{n,m}^{(HG)}(F, \upsilon, \zeta) = \sqrt{\frac{(2F-1)^{m+n}}{n!\, m!\, 2^{n+m}}}\, H_n\left(\frac{\sqrt{2}\, F\upsilon}{\sqrt{2F-1}}\right) H_m\left(\frac{\sqrt{2}F\zeta}{\sqrt{2F-1}}\right) F e^{-F\rho^2}, \tag{B3}$$

where n is the order of the Hermite polynomial H_n along y axis, m is the order along z axis, $\rho^2 = \upsilon^2 + \zeta^2$. Hermite polynomials verify

$$H_n(x) = 2x H_{n-1}(x) - 2(n-1) H_{n-2}(x), \tag{B4}$$

$$H_n''(x) - 2x H_n'(x) + 2n H_n(x) = 0, \tag{B5}$$

where $'$ accounts for the derivative with respect to the variable x and the first two polynomials are $H_0(x) = 1$ and $H_1(x) = 2x$.

Hermite-Gaussian propagation modes are orthogonal between one another, with the inner product defined by Eq. (C7):

$$\begin{aligned}\left\langle \psi_{n,m}^{(HG)}, \psi_{p,q}^{(HG)} \right\rangle &= \iint_{-\infty}^{+\infty} \psi_{n,m}^{(HG)}\, \bar{\psi}_{p,q}^{(HG)}\, d\upsilon\, d\zeta \\ &= \left\langle \psi_{p,q}^{(HG)}, \psi_{n,m}^{(HG)} \right\rangle = \iint_{-\infty}^{+\infty} \psi_{p,q}^{(HG)} \bar{\psi}_{n,m}^{(HG)}\, d\upsilon\, d\zeta \\ &= \frac{\pi}{2}\, \delta_n^p \delta_m^q,\end{aligned} \tag{B6}$$

where δ_n^p refers to Kronecker δ function and the symbol $\bar{}$ denotes the complex conjugate.

In the transverse-spatial Fourier space,the (n, m)-order Hermite-Gaussian mode reads

$$\hat{\psi}_{n,m}^{(HG)} = C_{n,m}^{(HG)}\, e^{-i\frac{\kappa_\perp^2}{4}\xi}, \tag{B7}$$

where

$$C_{n,m}^{(HG)} = \frac{(-i)^{n+m}}{4\pi\sqrt{n!\, m!\, 2^{n+m}}}\, H_n\left(\frac{\kappa_y}{\sqrt{2}}\right) H_m\left(\frac{\kappa_z}{\sqrt{2}}\right) e^{-\frac{\kappa_\perp^2}{4}}. \tag{B8}$$

Transverse derivatives of Hermite-Gaussian modes can be expressed as a linear combination of Hermite-Gaussian modes:

$$i\kappa_y \hat{\psi}^{(HG)}_{n,m} = -\sqrt{n+1}\,\hat{\psi}^{(HG)}_{n+1,m} + \sqrt{n}\,\hat{\psi}^{(HG)}_{n-1,m}, \tag{B9}$$

$$i\kappa_z \hat{\psi}^{(HG)}_{n,m} = -\sqrt{m+1}\,\hat{\psi}^{(HG)}_{n,m+1} + \sqrt{m}\,\hat{\psi}^{(HG)}_{n,m-1}, \tag{B10}$$

where, by notation convention, $\sqrt{n}\,H_{n-1}(x) = 0$ if $n = 0$.

2. Laguerre-Gaussian modes

The Laguerre-Gaussian modes are a well-known complete family of orthogonal paraxial solutions:

$$\psi^{(LG)}_{p,l}(F,\upsilon,\zeta) = \frac{(2F-1)^p(\sqrt{2}\,F)^{|l|}}{\sqrt{\frac{(p+|l|)!}{p!}}}(\upsilon + \mathrm{sgn}(l)\,i\zeta)^{|l|}L_p^{|l|} \times \left(\frac{2\rho^2F^2}{2F-1}\right)Fe^{-F\rho^2}, \tag{B11}$$

where $p \geqslant 0$ is the radial index and l is the azimuthal index (it can be negative, zero, or positive integer) of the generalized Laguerre polynomial $L_p^{|l|}$, and $\mathrm{sgn}(l)$ is the sign of l, i.e., $\mathrm{sgn}(l) = 1$ if $l \geqslant 0$ and $\mathrm{sgn}(l) = -1$ if $l < 0$. Generalized Laguerre polynomials verify

$$L_p^{|l|}(x) = \frac{(2p+|l|-1-x)L_{p-1}^{|l|}(x) - (p+|l|-1)L_{p-2}^{|l|}(x)}{p}, \tag{B12}$$

where the first two polynomials are $L_0^{|l|}(x) = 1$ and $L_1^{|l|}(x) = 1 + |l| - x$.

Laguerre-Gaussian propagation modes constitute an orthogonal set:

$$\left\langle \psi^{(LG)}_{p,l}, \psi^{(LG)}_{q,r} \right\rangle = \left\langle \psi^{(LG)}_{q,r}, \psi^{(LG)}_{p,l} \right\rangle = \frac{\pi}{2}\,\delta^q_p\delta^r_l. \tag{B13}$$

The Gaussian beam belongs to both Hermite-Gaussian and Laguerre-Gaussian families:

$$\phi^{(HG)}_{0,0} = \phi^{(LG)}_{0,0}. \tag{B14}$$

In the transverse-spatial Fourier space, the (p,l)-order Laguerre-Gaussian mode reads

$$\hat{\psi}^{(LG)}_{p,l} = C^{(LG)}_{l,p}\,e^{-i\frac{\kappa_\perp^2}{4}\xi}, \tag{B15}$$

where

$$C^{(LG)}_{p,l} = \frac{(-i)^{2p+|l|}\sqrt{p!}}{4\pi\sqrt{2^{|l|}(p+|l|)!}}(\kappa_y + \mathrm{sgn}(l)\,i\kappa_z)^{|l|}L_p^{|l|}\left(\frac{\kappa_\perp^2}{2}\right)e^{-\frac{\kappa_\perp^2}{4}}. \tag{B16}$$

Transverse derivatives of Laguerre-Gaussian modes can be expressed as a linear combination of Laguerre-Gaussian modes:

$$-\kappa_\perp^2\hat{\psi}^{(LG)}_{p,l} = -2(2p+|l|+1)\,\hat{\psi}^{(LG)}_{p,l} - 2\sqrt{(p+1)(p+1+|l|)}\,\hat{\psi}^{(LG)}_{p+1,l} - 2\sqrt{p(p+|l|)}\,\hat{\psi}^{(LG)}_{p-1,l}, \tag{B17}$$

where, by notation convention, $\sqrt{p}\,L_{p-1}^{|l|}(x) = 0$ if $p = 0$.

APPENDIX C: LASER POWER AND ENERGY TRANSPORTED THROUGH A TRANSVERSE PLANE AND DEFINITION OF THE INNER PRODUCT BETWEEN SPATIAL ENVELOPES

The Poynting vector is defined as

$$\boldsymbol{\Pi} = c^2\varepsilon_0(\boldsymbol{E} \times \bar{\boldsymbol{B}}), \tag{C1}$$

where the symbol $\bar{}$ denotes the complex conjugate. Its longitudinal component is

$$\Pi_x = c^2\varepsilon_0(E_y\bar{B}_z - E_z\bar{B}_y), \tag{C2}$$

whose integral over the transverse coordinates, calculated by employing Ansätze Eqs. (7) and (8), gives the power flux through the transverse planes:

$$P = \frac{c\varepsilon_0E_0^2D_0^2}{4}\iint_{-\infty}^{+\infty}\left(\psi_{E_y}\bar{\psi}_{B_z} - \psi_{E_z}\bar{\psi}_{B_y}\right)d\upsilon\,d\zeta. \tag{C3}$$

Integration of Eq. (C3) over time, assuming that there is a time-dependent envelope, gives the total laser energy, which should be the same through any transverse plane:

$$U = \frac{1}{\omega_0}\int_{-\infty}^{+\infty}P\,d\tau. \tag{C4}$$

The form of the integral in Eq. (C4) suggests us to define the following inner product of spatial envelopes:

$$\langle a,b\rangle := \iiint_{-\infty}^{+\infty}a\bar{b}\,d\upsilon\,d\zeta\,d\tau, \tag{C5}$$

which gives us the total energy of the laser pulse:

$$\frac{4\omega_0U}{c\varepsilon_0E_0^2D_0^2} = \left\langle\psi_{E_y},\psi_{B_z}\right\rangle - \left\langle\psi_{E_z},\psi_{B_y}\right\rangle. \tag{C6}$$

Note that for monochromatic beams (i.e., the envelopes do not depend on time) the inner product is defined as

$$\langle a,b\rangle := \iint_{-\infty}^{+\infty}a\bar{b}\,d\upsilon\,d\zeta, \tag{C7}$$

and, in this case, $\langle\psi_{E_y},\psi_{B_z}\rangle - \langle\psi_{E_z},\psi_{B_y}\rangle$ represents the total power flux through transverse planes:

$$\frac{4P}{c\varepsilon_0E_0^2D_0^2} = \left\langle\psi_{E_y},\psi_{B_z}\right\rangle - \left\langle\psi_{E_z},\psi_{B_y}\right\rangle. \tag{C8}$$

Following the definition of the inner product, if x is a scalar (i.e., it does not depend on υ and ζ), we have that

$$\langle xa,b\rangle = x\langle a,b\rangle, \tag{C9}$$

$$\langle a,xb\rangle = \bar{x}\langle a,b\rangle. \tag{C10}$$

Moreover, it follows from the theory of distributions that odd transverse-coordinate and time derivatives are anticommutative and even transverse-coordinate and time derivatives are commutative. For instance,

$$\langle \partial_\upsilon a, a\rangle = -\langle a, \partial_\upsilon a\rangle, \tag{C11}$$

$$\langle \partial_\upsilon^2 a, a\rangle = \langle a, \partial_\upsilon^2 a\rangle, \tag{C12}$$

provided that $a(\upsilon \to \pm\infty) = 0$ and $\partial_\upsilon a(\upsilon \to \pm\infty) = 0$.

APPENDIX D: THE EXACT MAXWELL SOLVER IN THE TRANSVERSE-SPATIAL FOURIER SPACE

We shall adapt the exact Maxwell solver in transverse-spatial Fourier domain of Ref. [32] to the spatial envelopes given in Ansätze Eqs. (7) and (8). Only the solver for monochromatic laser beams is presented here. To do so, those Ansätze are substituted into the Maxwell equations, and we obtain the following overdetermined system:

$$\begin{pmatrix} k_x & k_y & k_z & 0 & 0 & 0 \\ 0 & 0 & 0 & k_x & k_y & k_z \\ 0 & -k_z & k_y & -k_0 & 0 & 0 \\ k_z & 0 & -k_x & 0 & -k_0 & 0 \\ k_y & -k_x & 0 & 0 & 0 & k_0 \\ k_0 & 0 & 0 & 0 & -k_z & k_y \\ 0 & -k_0 & 0 & -k_z & 0 & k_x \\ 0 & 0 & k_0 & -k_y & k_x & 0 \end{pmatrix} \begin{pmatrix} \hat\psi_{E_x} \\ \hat\psi_{E_y} \\ \hat\psi_{E_z} \\ \hat\psi_{B_x} \\ \hat\psi_{B_y} \\ \hat\psi_{B_z} \end{pmatrix} = \mathbf{0}, \tag{D1}$$

where $k_x = \sqrt{k_0^2 - k_y^2 - k_z^2}$ is the longitudinal component of the wave vector. We only consider forward-propagating modes (i.e., $k_x \geqslant 0$), and hence we require $\hat\psi(x, k_y, k_z) = 0$ if $k_y^2 + k_z^2 > k_0^2$.

The system Eq. (D1) has a unique solution if we assume that the two transverse components of the electric field, E_y and E_z, are known:

$$\hat\psi_{E_x} = -\frac{k_y}{k_x}\hat\psi_{E_y} - \frac{k_z}{k_x}\hat\psi_{E_z}, \tag{D2}$$

$$\hat\psi_{B_x} = -\frac{k_z}{k_0}\hat\psi_{E_y} + \frac{k_y}{k_0}\hat\psi_{E_z}, \tag{D3}$$

$$\hat\psi_{B_y} = -\frac{k_y k_z}{k_0 k_x}\hat\psi_{E_y} - \frac{k_0^2 - k_y^2}{k_0 k_x}\hat\psi_{E_z}, \tag{D4}$$

$$\hat\psi_{B_z} = \frac{k_0^2 - k_z^2}{k_0 k_x}\hat\psi_{E_y} + \frac{k_y k_z}{k_0 k_x}\hat\psi_{E_z}. \tag{D5}$$

The transverse components of the electric field are prescribed in the transverse plane at $x = x_0$ and propagated according the following expression:

$$\hat\psi_{E_y}(x, k_y, k_z) = \hat\psi_{E_y}(x_0, k_y, k_z) e^{-i(k_0 - k_x)(x - x_0)}, \tag{D6}$$

$$\hat\psi_{E_z}(x, k_y, k_z) = \hat\psi_{E_z}(x_0, k_y, k_z) e^{-i(k_0 - k_x)(x - x_0)}, \tag{D7}$$

which is the exact forward-propagating solution of Eq. (12).

APPENDIX E: EXAMPLES OF ASYMPTOTIC EXPANSIONS (LEADING TERM)

1. Monochromatic Hermite-Gaussian beams

If n and m are both even integers, the (n, m)-order Hermite-Gaussian mode [see Eq. (B3)] behaves asymptotically where $\xi \to \pm\infty$, like

$$\psi_{n,m}^{(HG)} \sim \frac{1}{\xi}[a_0 + O(\xi^{-1})], \tag{E1}$$

$$a_0 = -\frac{i\,\pi\,\sqrt{n!\,m!}}{2^{\frac{n+m}{2}}\left(\frac{n}{2}\right)!\left(\frac{m}{2}\right)!}. \tag{E2}$$

If n is even and m is odd, then

$$\psi_{n,m}^{(HG)} \sim \frac{1}{\xi^2}[a_0 + O(\xi^{-1})], \tag{E3}$$

$$a_0 = -\frac{2\sqrt{2}\,\sqrt{n!\,m!}}{2^{\frac{n+m}{2}}\left(\frac{n}{2}\right)!\left(\frac{m-1}{2}\right)!}\,\zeta. \tag{E4}$$

If n is odd and m is even, then

$$\psi_{n,m}^{(HG)} \sim \frac{1}{\xi^2}[a_0 + O(\xi^{-1})], \tag{E5}$$

$$a_0 = -\frac{2\sqrt{2}\,\sqrt{n!\,m!}}{2^{\frac{n+m}{2}}\left(\frac{n-1}{2}\right)!\left(\frac{m}{2}\right)!}\,\upsilon. \tag{E6}$$

If both n and m are odd integers, then the asymptotic expansion is

$$\psi_{n,m}^{(HG)} \sim \frac{1}{\xi^3}[a_0 + O(\xi^{-1})], \tag{E7}$$

$$a_0 = \frac{8\,i\,\sqrt{n!\,m!}}{2^{\frac{n+m}{2}}\left(\frac{n-1}{2}\right)!\left(\frac{m-1}{2}\right)!}\,\upsilon\zeta. \tag{E8}$$

Whenever n and m are not simultaneously odd integers, by substituting Eqs. (E2), (E4), and (E6) into Eqs. (119) and (120) one deduces that the paraxial-order term dominates far from the focal plane:

$$\psi_{E_y}^{\infty} \sim \psi_{n,m}^{(HG)}, \tag{E9}$$

$$\psi_{E_z}^{\infty} \sim 0. \tag{E10}$$

When both n and m are odd integers, the substitution of Eq. (E8) into Eqs. (119) and (120) yields an extra term $\sim O(\xi^{-3})$ in the asymptotic limit of E_z:

$$\psi_{E_y}^{\infty} \sim \psi_{n,m}^{(HG)}, \tag{E11}$$

$$\psi_{E_z}^{\infty} \sim \frac{\varepsilon^2}{8\upsilon\zeta}\,\psi_{n,m}^{(HG)}. \tag{E12}$$

Following Eq. (112), it is straightforward to verify that these asymptotic limits contain all the power through the transverse plane of the solution.

2. Monochromatic Laguerre-Gaussian beams

Laguerre-Gaussian modes [see Eq. (B11)] behave asymptotically where $\xi \to \pm\infty$, like

$$\psi_{p,l}^{(LG)} \sim F^{|l|+1}[a_0 + O(\xi^{-1})], \tag{E13}$$

$$a_0 = \alpha_0\, \rho^{|l|} e^{il\phi}, \tag{E14}$$

$$\alpha_0 = (-1)^p \sqrt{\frac{2^{|l|}\, p!}{(p+|l|)!}} L_p^{|l|}(0), \tag{E15}$$

where $F = i/(i-\xi)$, $\rho e^{\pm i\phi} = \upsilon \pm i\zeta$, and, in the cylindrical coordinate system, $\rho = \sqrt{\upsilon^2+\zeta^2}$ represents the radial distance and ϕ is the azimuth (such that $\upsilon = \rho\cos\phi$ and $\zeta = \rho\sin\phi$). Note that $L_p^{|l|}(0) \neq 0$ for all $p \geqslant 0$ and l. After some manipulations, when substituting Eq. (E14) into Eqs. (119)–(122), we have

$$A_{E_y}^{(2)} = \frac{|l|(|l|-1)}{8}\alpha_0\,(\upsilon + i\,\mathrm{sgn}(l)\zeta)^{|l|-2}, \tag{E16}$$

$$A_{E_z}^{(2)} = \mathrm{sgn}(l) i\, A_{E_y}^{(2)}, \tag{E17}$$

which are zero if $|l| \leqslant 1$, and for $j > 1$,

$$A_{E_y}^{(2j)} = A_{E_z}^{(2j)} = 0. \tag{E18}$$

Therefore, the limits for E_y and E_z are, respectively,

$$\psi_{E_y}^{\infty} \sim \left[1 + \frac{\varepsilon^2 |l|(|l|-1)}{8(\upsilon + i\,\mathrm{sgn}(l)\zeta)^2}\right]\psi_{p,l}^{(LG)}, \tag{E19}$$

$$\psi_{E_z}^{\infty} \sim \frac{i\varepsilon^2 l(|l|-1)}{8(\upsilon + i\,\mathrm{sgn}(l)\zeta)^2}\psi_{p,l}^{(LG)}. \tag{E20}$$

3. Hermite-Gaussian laser pulses

In the transverse-spatial and temporal Fourier space, we multiply the (n,m)-order Hermite-Gaussian mode in the focal plane ($\xi = 0$) by a temporal envelope $C_\tau(\Omega)$, to prescribe the transverse fields according to Eqs. (112) and (113) with the following paraxial mode:

$$\hat{\psi}^{(0)} = C_\tau(\Omega)\, C_{n,m}^{(HG)}(\kappa_y, \kappa_z)\, e^{-i\frac{\kappa_\perp^2}{4\hat{T}}\xi}, \tag{E21}$$

which satisfies Eq. (B2) and where $C_{n,m}^{(HG)}$ is given by Eq. (B8). Since by this choice the temporal and transverse-spatial envelopes are separated in the focal plane, the inverse transverse-spatial Fourier transform of Eq. (E21) is straightforward and thus the paraxial mode in position space reads

$$\psi^{(0)} = \mathcal{F}_\tau^{-1}\big[C_\tau(\Omega)\, \psi_{n,m}^{(HG)}(\tilde{F}, \upsilon, \zeta)\big], \tag{E22}$$

where $\psi_{n,m}^{(HG)}$ is given by Eq. (B3) and

$$\tilde{F} = \frac{i}{i - \xi/\hat{T}}. \tag{E23}$$

Following Sec. E 1, whenever n and m are not simultaneously odd integers the asymptotic limits far from the focal plane are

$$\psi_{E_y}^{\infty} \sim \mathcal{F}_\tau^{-1}\big[C_\tau(\Omega)\, \psi_{n,m}^{(HG)}(\tilde{F}, \upsilon, \zeta)\big], \tag{E24}$$

$$\psi_{E_z}^{\infty} \sim 0. \tag{E25}$$

When both n and m are odd integers,

$$\psi_{E_y}^{\infty} \sim \mathcal{F}_\tau^{-1}\big[C_\tau(\Omega)\, \psi_{n,m}^{(HG)}(\tilde{F}, \upsilon, \zeta)\big], \tag{E26}$$

$$\psi_{E_z}^{\infty} \sim \frac{\varepsilon^2}{8T^2\upsilon\zeta}\, \mathcal{F}_\tau^{-1}\big[C_\tau(\Omega)\, \psi_{n,m}^{(HG)}(\tilde{F}, \upsilon, \zeta)\big]. \tag{E27}$$

4. Laguerre-Gaussian laser pulses

Analogously to Sec. E 3, we prescribe laser field components based on the following paraxial mode that comes from multiplying a time envelope by a Laguerre-Gaussian mode in the focal plane:

$$\psi^{(0)} = \mathcal{F}_\tau^{-1}\big[C_\tau(\Omega)\, \psi_{p,l}^{(LG)}(\tilde{F}, \upsilon, \zeta)\big], \tag{E28}$$

where $C_{p,l}^{(LG)}$ is given by Eq. (B16) and $\tilde{F}$ is given by Eq. (E23).

Following Sec. E 2, the asymptotic limits for each transverse laser components are, respectively,

$$\psi_{E_y}^{\infty} \sim \mathcal{F}_\tau^{-1}\big[C_\tau(\Omega)\, \psi_{p,l}^{(LG)}(\tilde{F}, \upsilon, \zeta)\big] \times \left[1 + \frac{\varepsilon^2 |l|(|l|-1)}{8T^2(\upsilon + i\,\mathrm{sgn}(l)\zeta)^2}\right], \tag{E29}$$

$$\psi_{E_z}^{\infty} \sim \mathcal{F}_\tau^{-1}\big[C_\tau(\Omega)\, \psi_{p,l}^{(LG)}(\tilde{F}, \upsilon, \zeta)\big] \times \frac{i\varepsilon^2 l(|l|-1)}{8T^2(\upsilon + i\,\mathrm{sgn}(l)\zeta)^2}. \tag{E30}$$

[1] K. M. Davis, K. Miura, N. Sugimoto, and K. Hirao, Opt. Lett. **21**, 1729 (1996).

[2] E. G. Gamaly, S. Juodkazis, K. Nishimura, H. Misawa, B. Luther-Davies, L. Hallo, P. Nicolai, and V. T. Tikhonchuk, Phys. Rev. B **73**, 214101 (2006).

[3] A. Patel, V. T. Tikhonchuk, J. Zhang, and P. G. Kazansky, Laser Photon. Rev. **11**, 1600290 (2017).

[4] A. G. Stepanov, J. Kuhl, I. Z. Kozma, E. Riedle, G. Almási, and J. Hebling, Opt. Express **13**, 5762 (2005).

[5] J. Hebling, K. L. Yeh, M. C. Hoffmann, B. Bartal, and K. A. Nelson, J. Opt. Soc. Am. B **25**, B6 (2008).

[6] W. R. Zipfel, R. M. Williams, and W. W. Webb, Nat. Biotechnol. **21**, 1369 (2003).

[7] S. H. Chung and E. Mazur, J. Biophotonics **2**, 557 (2009).

[8] C. K. Birdsall and A. B. Langdon, *Plasma Physics via Computer Simulation* (McGraw-Hill, New York, 1985).

[9] R. W. Hockney and J. W. Eastwood, *Computer Simulation Using Particles* (Adam Hilger, Bristol, 1988).

[10] M. Kolesik, J. V. Moloney, and M. Mlejnek, Phys. Rev. Lett. **89**, 283902 (2002).

[11] M. Kolesik and J. V. Moloney, Phys. Rev. E **70**, 036604 (2004).

[12] A. Couairon, O. G. Kosareva, N. A. Panov, D. E. Shipilo, V. A. Andreeva, V. Jukna, and F. Nesa, Opt. Express **23**, 31240 (2015).
[13] E. Esarey, P. Sprangle, M. Pilloff, and J. Krall, J. Opt. Soc. Am. B **12**, 1695 (1995).
[14] J.-X. Li, Y. I. Salamin, K. Z. Hatsagortsyan, and C. H. Keitel, J. Opt. Soc. Am. B **33**, 405 (2016).
[15] S. M. Sepke and D. P. Umstadter, Opt. Lett. **31**, 2589 (2006).
[16] V. Y. Fedorov, M. Chanal, D. Grojo, and S. Tzortzakis, Phys. Rev. Lett. **117**, 043902 (2016).
[17] V. Marceau, C. Varin, and M. Piché, Opt. Lett. **38**, 821 (2013).
[18] A. Martens, K. Dupraz, K. Cassou, N. Delerue, A. Variola, and F. Zomer, Opt. Lett. **39**, 981 (2014).
[19] M. Lax, W. H. Louisell, and W. B. McKnight, Phys. Rev. A **11**, 1365 (1975).
[20] L. W. Davis, Phys. Rev. A **19**, 1177 (1979).
[21] M. Couture and Pierre-A. Belanger, Phys. Rev. A **24**, 355 (1981).
[22] C. J. R. Sheppard and S. Saghafi, J. Opt. Soc. Am. A **16**, 1381 (1999).
[23] Y. I. Salamin, Appl. Phys. B **86**, 319 (2007).
[24] S. R. Seshadri, J. Opt. Soc. Am. A **25**, 2156 (2008).
[25] G. P. Agrawal and D. N. Pattanayak, J. Opt. Soc. Am. **69**, 575 (1979).
[26] G. P. Agrawal and M. Lax, Phys. Rev. A **27**, 1693 (1983).
[27] T. Takenaka, M. Yokota, and O. Fukumitsu, J. Opt. Soc. Am. A **2**, 826 (1985).
[28] H. Laabs, Opt. Commun. **147**, 1 (1997).
[29] M. A. Porras, Opt. Lett. **26**, 44 (2001).
[30] C. Varin, M. Piché, and M. A. Porras, J. Opt. Soc. Am. A **23**, 2027 (2006).
[31] P. Favier, K. Dupraz, K. Cassou, A. M. X. Liu, C. F. Ndiaye, T. Williams, and F. Zomer, J. Opt. Soc. Am. A **34**, 1351 (2017).
[32] I. Thiele, S. Skupin, and R. Nuter, J. Comput. Phys. **321**, 1110 (2016).
[33] K. S. Yee, IEEE Trans. Antennas Propag. **14**, 302 (1966).
[34] R. P. Cameron and S. M. Barnett, New J. Phys. **14**, 123019 (2012).
[35] L. Bergé, S. Skupin, R. Nuter, J. Kasparian, and J. P. Wolf, Rep. Prog. Phys. **70**, 1633 (2007).
[36] T. Brabec and F. Krausz, Phys. Rev. Lett. **78**, 3282 (1997).
[37] J. P. Gram, J. reine angew. Math. **94**, 41 (1883).
[38] E. Schmidt, Math. Ann. **63**, 433 (1907).
[39] C. Cohen-Tannoudji, B. Diu, and F. Laloë, *Mécanique Quantique I*, 2nd ed. (Hermannn-Éditeurs des Sciences et des Arts, Paris, France, 1998).
[40] C. Cohen-Tannoudji, B. Diu, and F. Laloë, *Mécanique Quantique II*, 2nd ed. (Hermannn-Éditeurs des Sciences et des Arts, Paris, France, 2000).
[41] I. Thiele, P. González de Alaiza Martínez, R. Nuter, A. Nguyen, L. Bergé, and S. Skupin, Phys. Rev. A **96**, 053814 (2017).
[42] J. P. Bérenger, J. Comput. Phys. **114**, 185 (1994).
[43] J. P. Bérenger, J. Comput. Phys. **127**, 363 (1996).
[44] A. Taflove and S. C. Hagness, *Computational Electrodynamics: The Finite-Difference Time-Domain Method*, 3rd ed. (Artech House, Boston, 2005).
[45] M. A. Bandres and J. C. Gutiérrez-Vega, Opt. Lett. **29**, 144 (2004).